Mantle Deformation Patterns Beneath the Central India Tectonic Zone: Evidence from SK(K)S Splitting Measurements in the Satpura Gondwana Basin and Adjacent Areas

Nitarani Bishoyi [1], Arun Kumar Dubey [1], and Ashwani Kant Tiwari [1]

[1]Department of Earth and Environmental Sciences, Indian Institute of Science Education and Research Bhopal - 462066, India

Correspondence: Ashwani Kant Tiwari (aktiwari@iiserb.ac.in)

Abstract. This study presents shear wave splitting (SWS) estimates for core-refracted SK(K)S phases utilizing data from nine seismic stations in the Central Indian Tectonic Zone (CITZ) that were temporarily operational between July 2023 and July 2025. The CITZ was formed during the Mesoproterozoic orogeny in central India, resulting from the collision of the northern Bundelkhand Craton with a jumble of South Indian cratons. We used transverse energy minimization methodology to ascertain the SWS parameters, the fast polarization directions (FPDs) and splitting delay times (δt). A total of 129 high-quality SWS measurements were obtained from 87 earthquakes (M>5.5) at epicentral distances between 84°-145° for SKS phases and 84°-180° for SKKS phases. The mean δts at each seismic station ranges from 0.7 to 1.4 seconds, demonstrating the upper mantle heterogeneity in the study region. Most stations show NE-SW FPDs, aligning with the Absolute Plate Motion (APM) of the Indian plate. Fresnel zone analysis suggests that 235 km is a promising average depth of anisotropy, indicating that the primary source of the observed SWS measurement is mantle flow at asthenospheric depths, rather than frozen lithospheric fabric. The difference between mean FPD and APM direction at some stations suggests the presence of fossilized anisotropic fabrics resulting from prior orogenic events during the Mesoproterozoic Era. Seismic stations near the Deccan Volcanic Province and mantle dyke zones have lower δt (<1 second) values, indicating significant magmatism during the Cretaceous period. Our findings suggest that the mantle flow beneath the CITZ is affected by both the present APM direction of the Indian plate and lithospheric frozen anisotropy resulting from prior Mesoproterozoic orogeny and Cretaceous mantle plume activity.

1 Introduction

The Earth's mantle, a dynamic and heterogeneous layer, is critical to the geodynamic evolution of our planet. Understanding its deformation patterns is essential for unraveling the tectonic history and present-day geodynamics of any region. The tectonic history of the Indian landmass spans the formation of ancient cratons, incorporation into supercontinents such as Rodinia and Gondwana, and eventual collision with Eurasia (Rao and Reddy, 2002; Rogers and Santosh, 2003, 2009; Mandal et al., 2013), resulting in some of the most prominent geological features. Geochronological, geological, and paleomagnetic data suggests that multiple continental blocks came together during the Proterozoic era, leading to the formation of two major supercontinents (Zhao et al., 2004). The first, Columbia, formed around 1.8 billion years ago (Hou et al., 2008), while the second, Rodinia, emerged around 1.0 billion years ago (Li et al., 2008). One significant feature of these ancient tectonic events within

the Indian shield is the presence of a Mesoproterozoic orogenic belt that runs in the ENE-WSW direction (Acharya, 1997; Acharyya, 2003). This collisional zone, known as the Central Indian Tectonic Zone (CITZ) or Satpura Orogen, is an important suture zone where continental fragments collided and amalgamated during the Mesoproterozoic Era.

The CITZ is a suture zone that demarcates the boundary between the northern and southern Indian cratons (Figure 1). It originated during the Mesoproterozoic orogeny in central India, when the northern Bundelkhand Craton collided with a disordered group of South Indian cratons (Bastar, Dharwar, and Singhbhum cratons) (Radhakrishna and Ramakrishnan, 1988; Radhakrishna, 1989; Radhakrishna and Naqvi, 1986; Tewari, 2001). However, the accretion timing and the kinematics of convergence between the northern and southern Indian cratons are still debated (Bhowmik et al., 2012; Roy and Prasad, 2003; Bora and Kumar, 2015). Some hypotheses propose that the southern Indian cratons underthrust northward beneath the northern Indian craton (Roy and Prasad, 2003; Mall et al., 2008; Mandal et al., 2013; Chattopadhyay et al., 2017), while others propose the opposite, with southward-directed underthrusting of the northern Indian craton beneath the southern Indian cratons (Acharyya, 2003; Mall et al., 2008; Bora and Kumar, 2015). Furthermore, recent research has shown the likelihood of double-sided subduction in the central region (Naganjaneyulu and Santosh, 2010; Deshmukh and Prabhakar, 2020), which would involve processes such as slab breakoff and subduction polarity reversal. The CITZ has thus been a focal point of several tectonic activities, including continental collision, subduction, and mantle deformation. In addition to these Proterozoic tectonic processes, the central India was subsequently modified by the Reunion mantle plume activity during the late Cretaceous ($\sim$66 Ma) (Richards et al. 1989, Sheth 2005, Chenet 2008). Mantle plumes are commonly interpreted as thermochemical upwellings that originated near the core-mantle boundary that can generate extensive decompression melting, causing significant modification of the lithosphere (Morgan, 1971). The reunion plume triggered not only the Deccan traps but also major lithospheric thinning and anisotropic fabric alterations (Barruol et al., 2019). Such plume -lithosphere interaction is likely to result in modifications that potentially overprints pre-existing Proterozoic tectonic fabrics within the CITZ region.

The Central Indian Suture (CIS) and the Southeast Sakoli Shear (SES) form the southern limit of the CITZ, while the Son Narmada North Fault (SNNF) defines the northern boundary (Figure 1). The numerous main faults that exist within these borders are the Son Narmada South Fault (SNSF), Barwani Sukta Fault (BSF), Gavligarh Fault (GF), Tapti Fault (TF), and Tan Shear (TS) (Figure 1, Kaila and Krishna (1992); Narula et al. (2000); Bhandari et al. (2011)). These fault systems highlight the dynamic character of tectonic interactions and accompanying deformation within the CITZ, contributing to the evolving structural framework of this geologically active zone.

Seismic anisotropy, caused by the directional dependence of seismic wave velocities, can be used to effectively define crustal and upper mantle deformation (Bowman and Ando, 1987; Vinnik et al., 1989; Silver and Chan, 1991; Savage, 1999). Seismic anisotropy can be explained by two main deformation mechanisms: shape preferred orientation (SPO) and lattice preferred orientation (LPO) (e.g., Savage (1999); Fouch and Rondenay (2006)). Crustal anisotropy is commonly attributed to LPO in mica-rich minerals such as biotite and amphibole, as well as SPO in cracks, fractures, and compositional layering formed

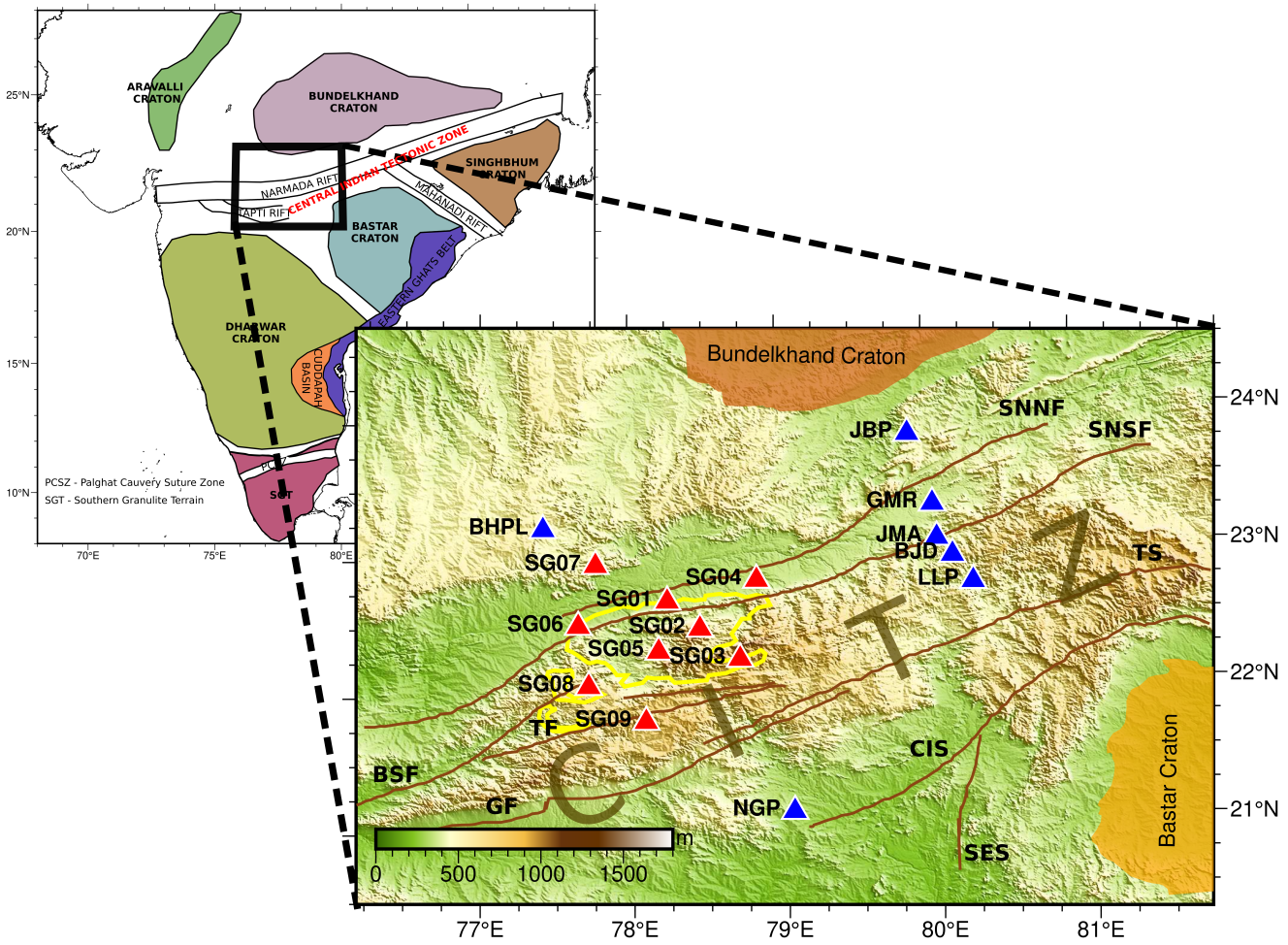


Figure 1. Tectonic and topographic map of the Central Indian Tectonic Zone across the Satpura Gondwana Basin. Red triangles denote the temporary seismic stations installed in and around the Satpura Gondwana Basin, whereas blue triangles indicate the seismic stations reported by Roy et al. (2014) and Roy et al. (2024). The fault lines shown in brown and the yellow curved lines denoting the boundary of the Satpura Gondwana Basin are adopted from Singh et al. (2015). Top Left: Regional geological and tectonic setting of Peninsular India, highlighting the distribution of Archean cratonic blocks and Proterozoic mobile belts (modified after Groves and Santosh, 2021). BSF: Barwani Sukta Fault; CIS: Central Indian Suture; GF: Gavligarh Fault; SNNF: Son Narmada North Fault; SNSF: Son Narmada South Fault; TF: Tapti Fault; TS: Tan Shear; SES: Sakoli East Shear.

during deformation (Crampin, 1984; Mainprice and Nicolas, 1989; Meissner et al., 2002; Fouch and Rondenay, 2006). Upper crustal anisotropy is primarily caused by structural features such as faults, layering, flat mineral alignment, and consistently oriented cracks in the upper crust (Crampin, 1984; Mainprice et al., 2000; Brownlee et al., 2017). The LPO of mica or amphibole minerals can explain anisotropy below the crack closure depth in the mid- to lower crust (Brownlee et al., 2017). Upper mantle seismic anisotropy is primarily attributed to the strain-induced LPO of anisotropic minerals, like olivine, orthopyroxene, and clinopyroxene, arising from the dislocation creep deformation mechanism, which is characterized by the creeping motion of crystal dislocations caused by mantle flow and tectonic stresses at the plate boundaries due to past and ongoing deformations (Karato, 1987; Barruol and Mainprice, 1993; Mainprice et al., 2000). Anisotropy in subduction zones may reflect fossilized fabrics in the overriding plate or stress-aligned crack systems influenced by slab dehydration and fluid migration, whereas in collisional orogens it is frequently associated with ductile shearing and lithospheric shortening, which produce coherent mineral fabrics parallel to orogenic trends (Savage, 1999; Long and Silver, 2009). In contrast, rift settings show anisotropy linked with extensional strain fields, with vertically aligned cracks and dike intrusions producing different anisotropic signatures.

Shear wave splitting (SWS) analysis of SK(K)S core-refracted phases is used globally to quantify seismic anisotropy. SK(K)S splitting measurements at any seismic station provide the integrated seismic anisotropy of the crust and upper mantle. When a shear wave travels across an anisotropic media, it splits into two pseudo "fast" and "slow" S-waves that travel in perpendicular directions with different wave speeds (Saltzer et al., 2000; Savage, 1999). SWS measurements provide seismic anisotropy parameters, polarization azimuth of the fast wave (fast polarization direction (ϕ or FPD)), and time difference between fast and slow wave (delay time (δt)), which provides critical information regarding strain patterns, mantle flow, and mechanical behavior of the lithosphere and sub-lithospheric system on the receiver side, allowing for inferences about mantle convection and tectonic history of the region (Silver and Chan, 1991; Barruol and Mainprice, 1993; Savage, 1999; Long and Silver, 2009).

A multitude of seismological investigations have been performed to elucidate the evolution and formation mechanisms of various regions in India by examining seismic anisotropy (Kumar and Singh, 2008; Paul et al., 2017; Biswal et al., 2020; Jana et al., 2021; Roy et al., 2021; Kanaujia and Surve, 2024; Roy et al., 2024) and its direct correlation to mantle deformation patterns, whether arising from present-day plate motion or the cumulative impact of prior and present-day orogenic events. Shear wave splitting has been extensively studied in the Himalayan region (northern India) to comprehend crustal and mantle deformation linked to the India-Eurasia collision (Paul et al., 2017; Kanaujia et al., 2019; Biswal et al., 2020). Similarly, numerous research studies on seismic anisotropy and its implications for lithospheric deformation have been performed in southern India (Roy et al., 2012; Kumar et al., 2015b; Sivaram et al., 2022) to better understand the evolution and formation mechanism of the southern Indian cratons. The SWS study has also highlighted the geological complexities of northeastern and eastern India (Bhukta et al., 2018; Singh et al., 2019). A recent study on seismic anisotropy across the whole Indian region (Roy et al., 2024) found that anisotropy in central India is caused by both frozen-in anisotropy and the shearing of the upper asthenosphere. Despite extensive research in these areas, the CITZ has received relatively less focus, despite its substantial

95 importance. Due to a shortage of seismic stations, the region has minimal seismological data, and no extensive SWS study has been undertaken in this area (Figure 2). Figure 2 shows the previously conducted splitting measurements for all of India (represented by blue bars) alongside our study region (grey-shaded area), thereby addressing the data deficiency in central India. The CITZ region experienced subduction-accretion-collision tectonics during the Mesoproterozoic era and mantle plume activity during the Cretaceous period, resulting in the formation of Peninsular India (Mall et al., 2008; Mandal et al., 2013; Kumar
100 et al., 2015a). Given its importance as a collisional zone, it is critical to investigate seismic anisotropy in this region to understand the deformation mechanisms. This study examines teleseismic SK(K)S waveform data collected from nine temporarily deployed broadband seismic stations in the CITZ region to assess the seismic anisotropy of the upper mantle at each station. We employed transverse energy minimization methodology to determine the SWS parameters. The resultant SWS parameters provide new insights into the deformational architecture of the crust and upper mantle in the study area. A comprehensive
105 geodynamic model for the CITZ is presented to elucidate the observed SWS patterns, which reveal the tectonic context and mantle deformation mechanisms responsible for the anisotropy beneath the region.

2 Data and Methodology

We utilize broadband seismic data collected from nine portable seismic stations that were operational from July 2023 to July
110 2025 (Figure 1). The seismic stations, equipped with Trillium Compact broadband seismometers, were deployed in three phases, with three stations installed in each phase. The earthquakes, having magnitudes exceeding 5.5, have been chosen for the SKS phase occurring within the epicentral distance ranges of 84° - 145° and for the SKKS phase, 84° - 180° (Figure 3). We have 424 teleseismic earthquakes based on magnitude and epicentral distance criteria, which were analyzed for SK(K)S-derived seismic anisotropy for all seismic stations. A band-pass filter having lower and higher cutoff frequencies of 0.05 Hz
115 and 0.2 Hz, respectively, is subsequently employed to enhance the SK(K)S seismic phases.

The SWS measurements were performed using the SplitLab (Wüstefeld et al., 2008), a software package developed in MATLAB. SplitLab offers multiple splitting algorithms to determine the optimal SWS parameters, ϕ and δt. To ensure the reliability of SWS parameters, we employ two distinct and independent methodologies: rotation correlation and transverse energy mini-
120 mization. The rotation correlation (RC) method (Bowman and Ando, 1987) determines the parameters ϕ and δt by finding the orientation that results in the highest correlation between the calculated fast and slow shear wave components. This method, however, may result in systematic inaccuracies, especially when the initial polarization aligns closely with the polarization of the fast or slow direction of the anisotropic media. Although predictable and well-documented, these errors can be accounted for to retrieve accurate splitting parameters.

125

The transverse energy minimization (TEM) technique (Silver and Chan, 1991) calculates ϕ and δt by minimizing the energy on the transverse component after applying the SWS correction. The TEM approach is generally considered more robust for

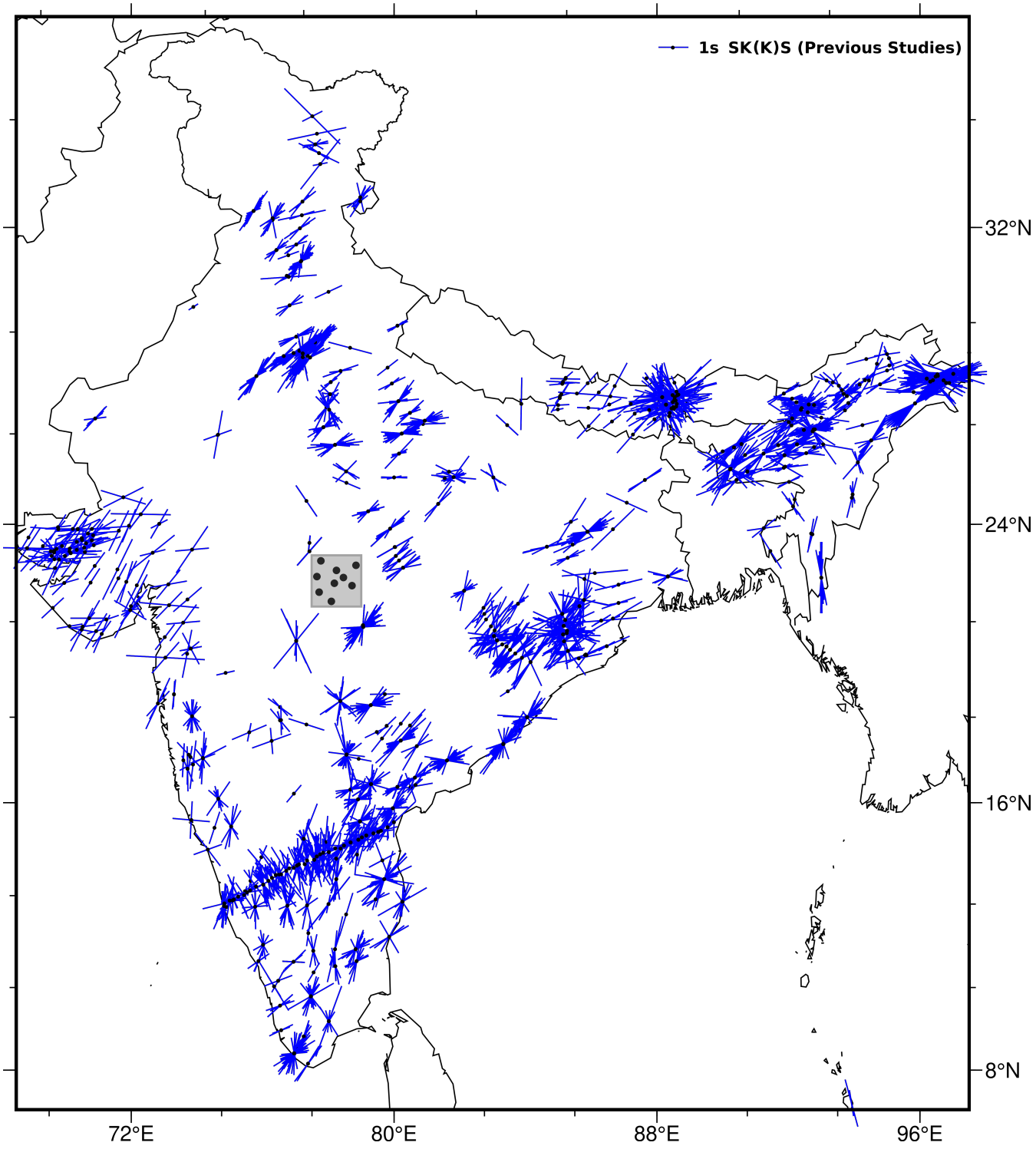


Figure 2. The figure illustrates the earlier SK(K)S-derived seismic anisotropy for the Indian region, depicted in blue (http://ds.iris.edu/spud/swsmeasurement), alongside our seismic stations, indicated in black circles. The bar length representing data at each seismic station corresponds to the δts , while their orientation indicates the FPDs.

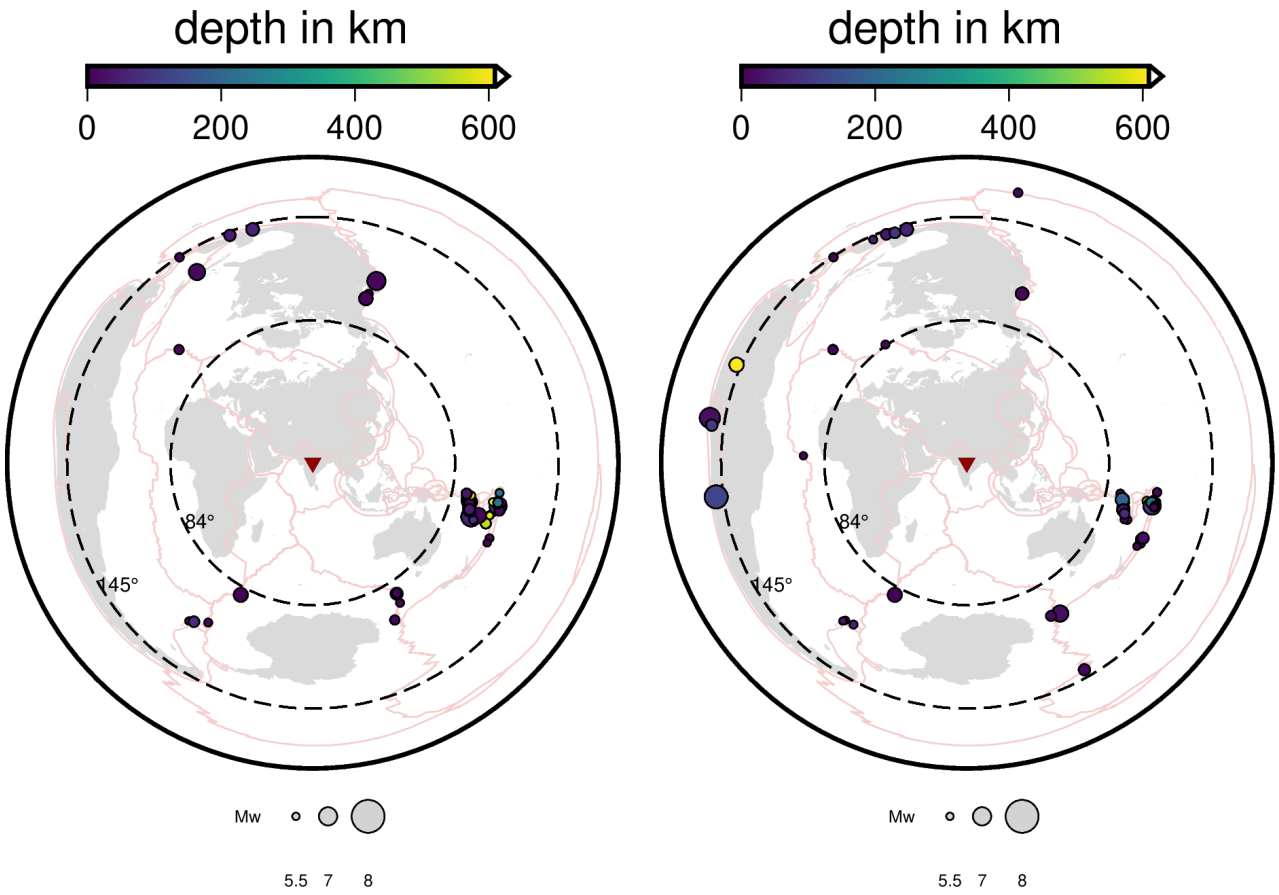


Figure 3. The epicentral distribution of earthquake events for (a) SKS (84° - 145°) and (b) SKKS (84° - 180°) seismic phases. The inverted dark red triangle represents the central location of seismic stations, while the circles denote earthquake events. The variation in circle colour indicates the depth of the earthquake events, while the size differences correspond to their magnitude.

SKS splitting measurements over a wide range of back azimuths. However, systematic errors, similar to those found in the RC approach, may have an impact, especially in circumstances with modest signal-to-noise ratios. This method assumes a single homogenous anisotropic layer and transverse isotropy with a horizontal symmetry axis. The TEM method follows a grid-search approach to ascertain the final optimal splitting parameter, which helps in determining the reliability of the results obtained from the TEM method. It accounts for potential fluctuations, likely induced by data noise, by providing a confidence level for each splitting parameter. Consequently, the findings presented in this study are primarily based on the TEM method.

Figure 4 shows an example of the SKS-derived good splitting measurement recorded at station SG01. The high-quality split event demonstrates a corrected particle motion with a good overlap between the fast and slow components (Figure 4). Before correction, the particle motion exhibits an elliptical trajectory; however, after correction, it takes a linear path that corresponds to the back azimuth (Figure 4). The transverse energy nears zero in the adjusted transverse component plot, and the splitting parameters ϕ and δt are consistent, with ϕ agreeing within 10° across several methods and δt within 0.2 seconds (Figure 4). Figure 5 shows an example of the SKKS derived splitting measurements at stations SG01. Figure 6 shows an example of a null measurement at the SG02 seismic station, in which particle motion before and after correction coincides and aligns linearly with the back-azimuth. In such cases, the energy of the transverse component is at a minimum. Null measurements, which show negligible tangential (SH) energy, may occur in three situations. The first occurs when no anisotropy is encountered and the initial SV polarization of the SK(K)S phases is unaffected by anisotropy. It appears practically impossible that any tectonic plate is isotropic in nature. Second, if the region is isotropic in nature due to complex anisotropy (multiple horizontal anisotropic layers with different fast polarization directions). Third, if the initial SV polarization is similar to that of the slow/fast anisotropy axis, the shear wave will not be split into two quasi-S waves (Saltzer et al., 2000; Barruol et al., 1997; Wüstefeld et al., 2008).

To ensure accurate SK(K)S splitting measurements, we performed a post-analysis verification of station orientation using the polarization characteristics of SK(K)S phases. For each event, we manually checked the particle motion before and after splitting correction. In particular, we compared the corrected radial component particle motion to the theoretical backazimuth of the incoming wave. After applying the splitting correction, the particle motion is expected to align with the source polarization direction, which coincides with the backazimuth (Liu and Gao, 2011; Eakin et al., 2018, 2019). For all final split datasets, the corrected particle motion projected onto the radial-transverse plane consistently aligns with the theoretical backazimuth, confirming that the stations are properly oriented and that orientation errors are minimal.

3 Results

After completing the splitting analysis, we have 129 reliable splitting measures, including 82 SKS splitting measurements and 47 SKKS splitting measurements. Supplementary Table S1 contains detailed information about the earthquake events (event

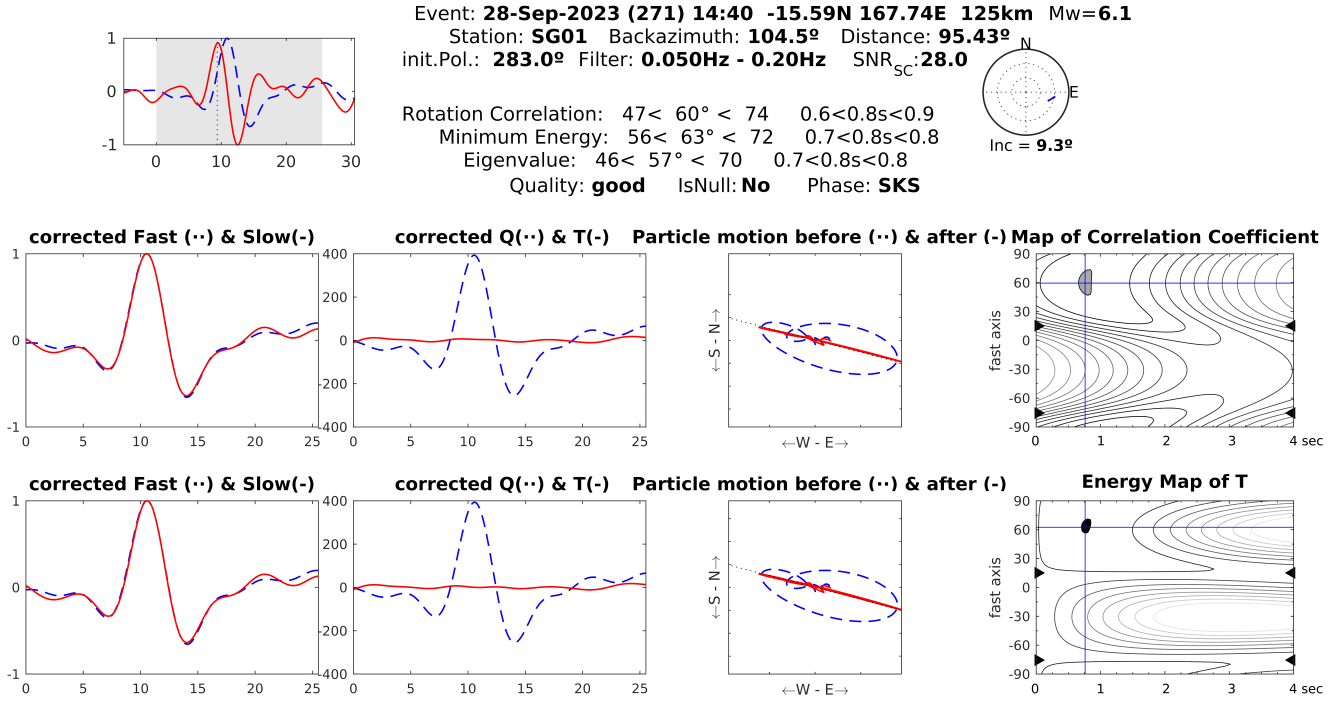


Figure 4. An example of a good SKS splitting phase for an earthquake recorded by the SG01 seismic station. The upper left graphic displays the radial component (blue dotted) and transverse (red solid) component, with the chosen time frame highlighted in gray. The top bar displays the event, station, and computed result information simultaneously. The stereoplot is shown in the top right corner. The second row presents the outcomes of the rotation-correlation (RC) method, including SKS fast directions (blue dashed) and slow ones (red solid) after RC delay correction; radial (blue dashed, Q) and transverse (red solid, T) components after RC delay correction; particle motion before (blue dashed) and after (red solid) RC delay correction; and a map of correlation coefficients. The third row displays the results of the transverse energy minimization technique. The descriptions are similar to the RC plots.

date, time, longitude, depth, and magnitude), station name, phase information, and shear wave splitting parameters with associated error (ϕ or FPD, FPD error, δt, and δt error) for each splitting measurement. We found six null measurements in our dataset, four at the SG02 seismic station and two at SG09. Supplementary Figure S1 shows a rose diagram of the backazimuthal coverage for the splits (in black) and the nulls (in red) for the SG02 and SG09 stations, demonstrating that the null and split measurements are obtained from different backazimuths, but their numbers are limited, so detailed modelling is the fundamental limitation of this study.

The majority of the analysed earthquakes are located in the back-azimuth range of 90° to 120° (Figure 7c), a constraint imposed by India's geographic position relative to the global distribution of large teleseismic earthquakes at appropriate epicentral distances. This narrow window is a well-documented limitation of SK(K)S splitting studies on the Indian subcontinent (Roy et al., 2012, 2014). Figure 7 shows a histogram of individual splitting parameters, demonstrating a predominant concentration of FPDs at 40° and δt around 0.85 - 1.1 seconds. The backazimuthal variation of individual FPDs observed at all seismic

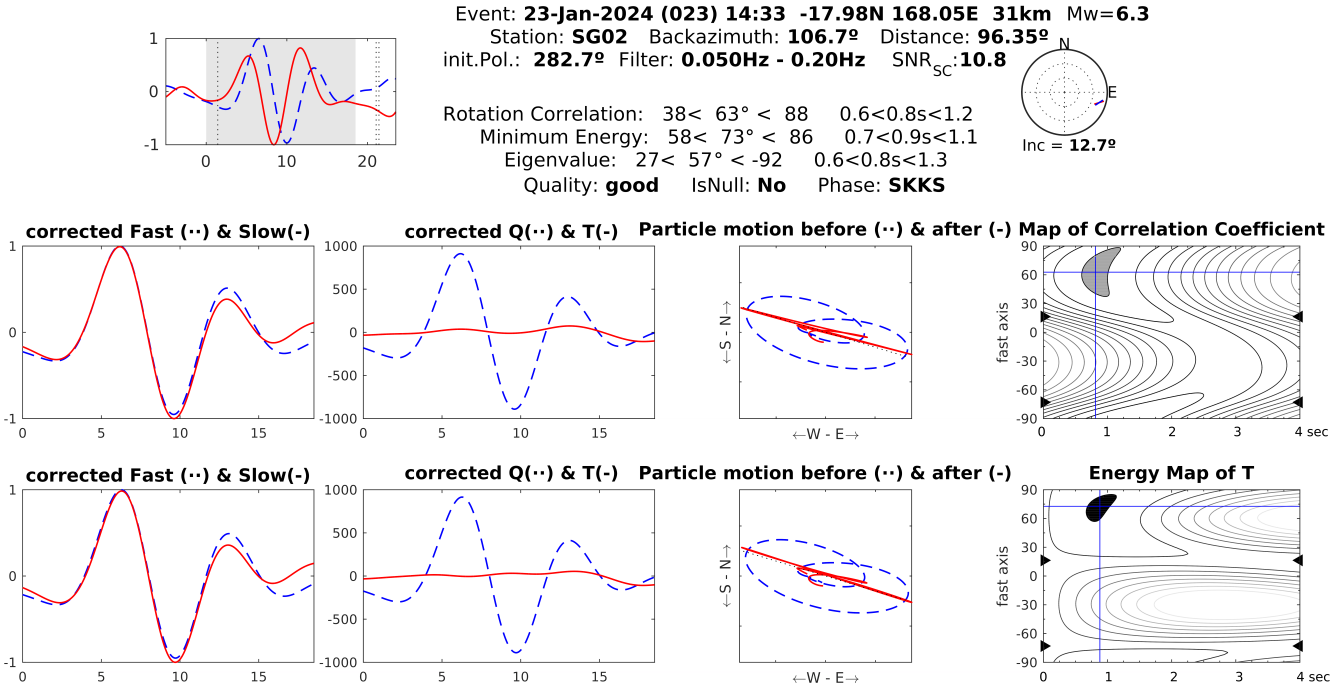


Figure 5. An instance of good SKKS-derived splitting measurement for an event recorded by the SG02 seismic station. The description corresponds identically to Figure 5.

stations (Figure 7c) indicates the existence of multiple anisotropic strata. However, the number of high-quality SKS measurements per station in our dataset is relatively limited, and backazimuthal coverage remains constrained (Supplementary Figure S2). Constructing meaningful splitting parameters versus backazimuth plots requires dense and well-distributed backazimuthal sampling, ideally spanning at least 180° with adequate event density in each bin, which is not uniformly achievable across all stations in our network. Splitting parameters for two layers of anisotropy modeling, whether at individual stations or station groups, can only be interpreted reliably when the variation of splitting parameters with backazimuth demonstrates a clear 90° periodicity (Silver and Savage, 1994; Savage, 1999). Ritter et al. (2022); Fröhlich et al. (2024) have explicitly demonstrated that when measurements are concentrated in a narrow backazimuthal range, layered models produce statistically indistinguishable fits, making unique structural determination impossible. Given these limitations, we have chosen not to proceed with two-layer anisotropy modeling in this study.

After calculating individual SK(K)S splitting measurements, the station-averaged splitting parameter for each station is calculated by averaging all splitting parameters derived from numerous events. The von Mises approach (Cochran et al., 2003) was used to calculate the circular mean of ϕ, whereas station-averaged δt was calculated using the arithmetic mean. The station-averaged SK(K)S splitting parameter for each seismic station is shown in Table 1. The average splitting δt at each station vary from 0.74 to 1.4 seconds (Figure 8). We have the lowest value of δt at the SG02 seismic station. Stations SG01, SG03, SG04,

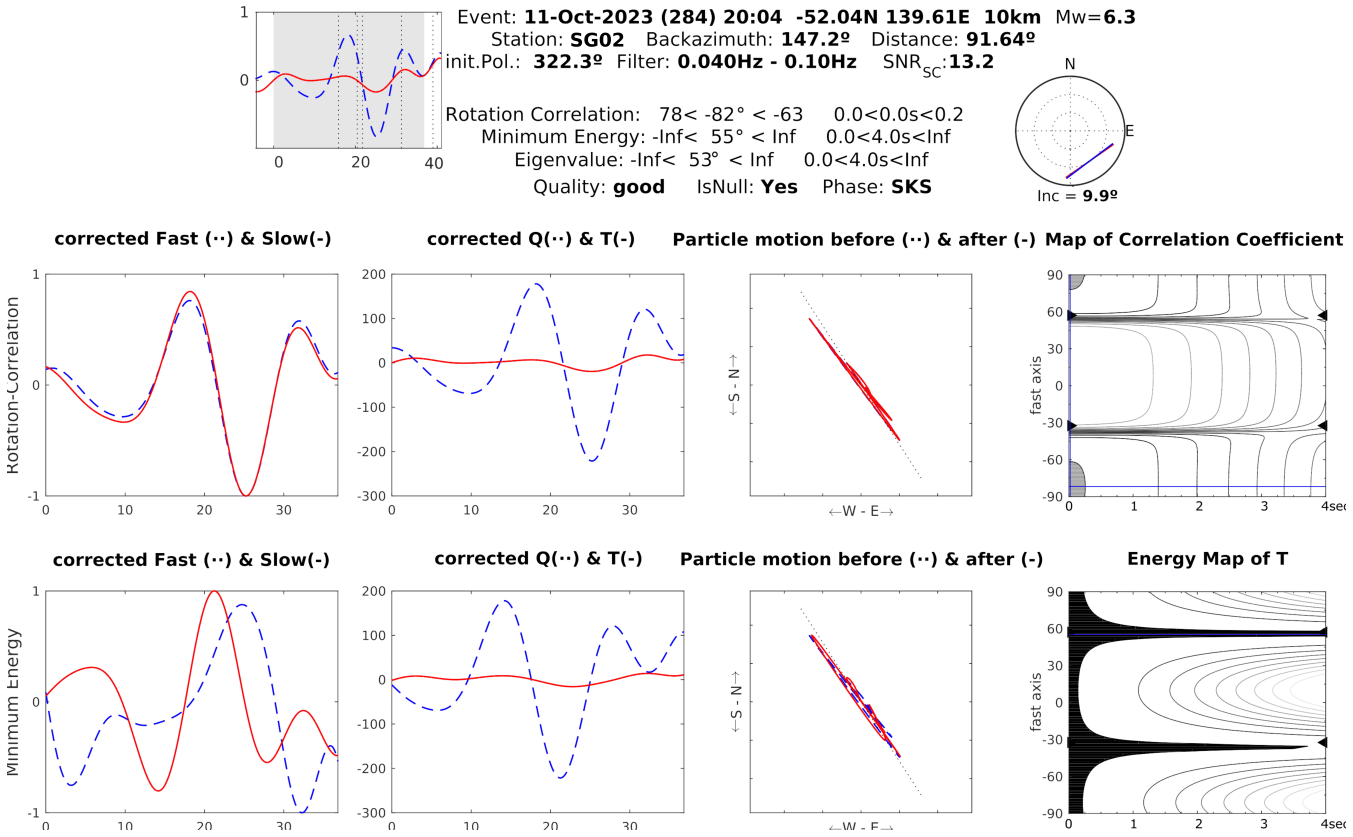


Figure 6. An example of null measurement at SG02 seismic station. The description corresponds identically to Figure 4.

SG05, and SG08 show high anisotropy (> 1 s), while stations SG02, SG06, SG07, and SG09 have low δt (< 1 s). The FPD values across all stations range from 24.84° (SG06 seismic station) to 70.88° (SG03 seismic station). Most seismic stations have a predominant NE-SW alignment of FPDs, which correlates closely to the Absolute Plate Motion (APM) direction of the Indian Plate (https://www.unavco.org/software/geodetic-utilities/plate-motion-calculator/plate-motion-calculator.html) with the ITRF2020 model (Altamimi et al., 2023) in the no-net-rotation frame of reference.

SK(K)S phases are typically considered to be near-vertical incident at seismic stations, therefore, the measurements are characterized by poor depth resolution (babuska 1991). Furthermore, to add depth constraints to the observed SKS splitting parameters, we conducted a Fresnel zone analysis based on the spatial coherency analysis of the high-quality SK(K)S splitting measurements (Liu and Gao, 2011; Gao and Liu, 2012). In the case of steep incident angles, the ray-path information is used to calculate the ray-piercing point at any assumed depth of the anisotropic layer. The mean splitting information is thus computed within the Fresnel zone, with the ray-piercing point as the center. The search for anisotropy depth was carried out at 5 km intervals within the depth range of 0-400 km. The variation factor is calculated as the weighted sum of the circular mean of the FPDs and the arithmetic mean of the splitting time delays. The depth value with the least variation factor was chosen as

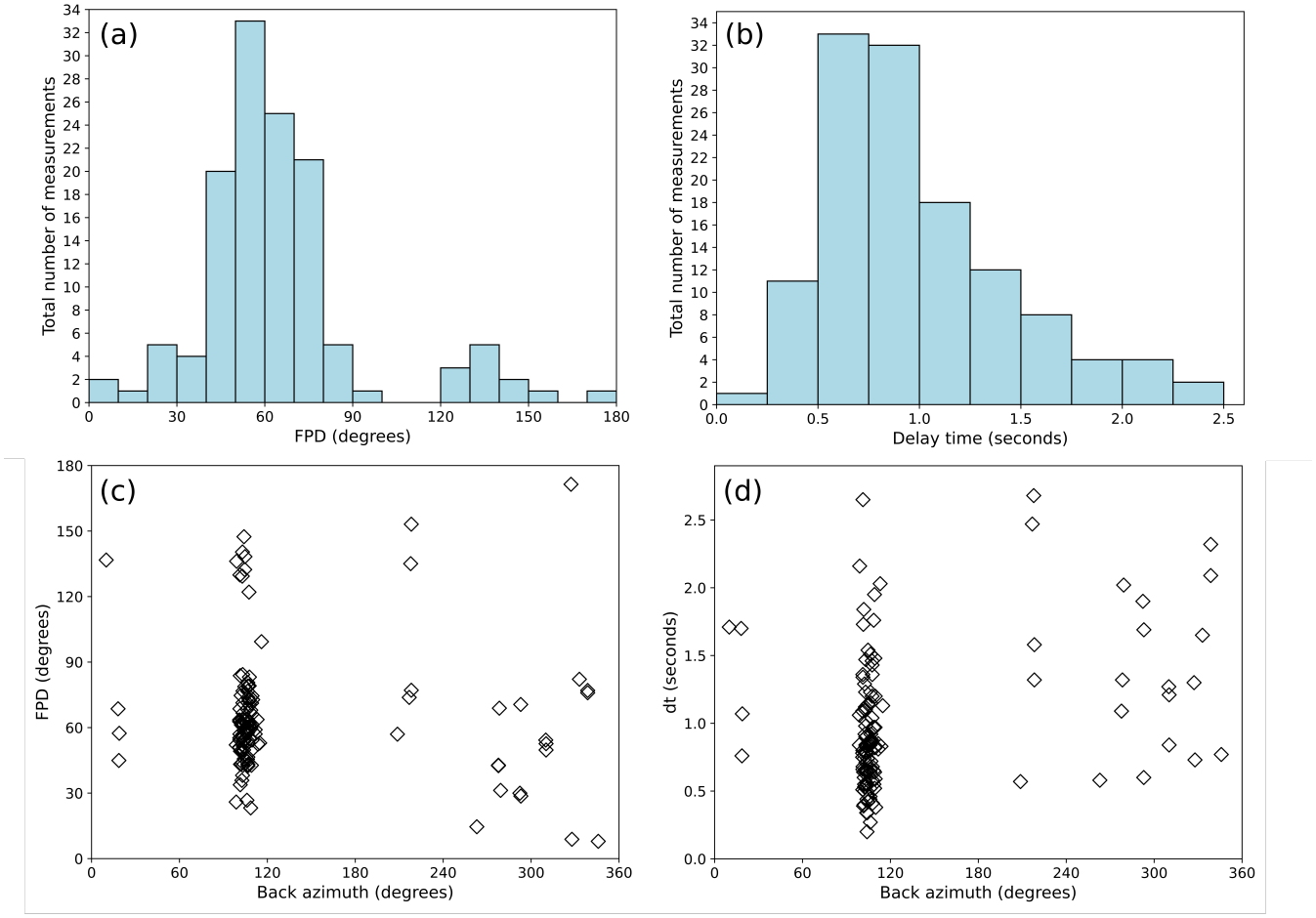


Figure 7. Histograms illustrating individual splitting parameters: (a) fast polarization directions (FPDs) and (b) delay times (δt). (c) and (d) illustrate the back azimuthal variation of individual FPDs and δts across all seismic stations, respectively. The majority of splitting measurements are concentrated within the backazimuthal range of 90° to 120°.

the optimal depth of the anisotropy. The variation factor was calculated at each depth for block sizes ranging from 0.05° to 4.0°, with an incremental interval of 0.05°. The optimum number of splitting measurements and spatial consistency in each block affect the variation factor. Both block-size configurations (dx = 0.30° and dx = 0.35°) show consistent behavior, with the variation factor declining steeply from near-surface values (∼0.95-1.0) down to a broad minimum in the 200-250 km depth range before stabilizing at ∼0.3-0.4 for greater depths. Figure 11 depicts the variation factor with varying anisotropic depth for block sizes of 0.30 and 0.35, indicating that 235 km represents a promising average depth of anisotropy. Our study found that the variation factor curve gradually flattens beyond ∼250 km, indicating that the technique's sensitivity decreases as depth increases and ray-piercing point separations become larger than the spatial scale of anisotropy variations. Supplementary Figure S4 in the revised manuscript demonstrates the piercing points at 50, 100, 200, and 300 km depth. The spatial distribution of ray-piercing points exhibits progressive lateral migration with increasing depth, which is consistent with the expected geometry of steeply incident SK(K)S raypaths. Individual Fresnel zone analysis for each seismic station was attempted, but the split measurements were insufficient to produce an acceptable result.

Table 1. Details of seismic stations, with averaged splitting parameters (FPD and δt).

Station	Lat (°)	Long (°)	Operation time		Station-averaged splitting parameters		No. of SK(K)S measurements
			Start date	End date	ϕ (°)	δt (s)	
SG01	22.70448	78.24171	16-07-2023	29-02-2024	43.90	1.08	13
SG02	22.50137	78.45606	17-07-2023	02-03-2024	56.49	0.74	19
SG03	22.27442	78.71826	18-07-2023	02-03-2024	70.88	1.04	13
SG04	22.84751	78.83887	02-03-2024	05-10-2024	34.61	1.42	16
SG05	22.34044	78.18029	03-03-2024	05-10-2024	47.70	1.29	19
SG06	22.52954	77.64957	03-03-2024	05-10-2024	24.84	0.90	15
SG07	22.97337	77.76826	06-10-2024	24-07-2025	59.66	0.88	10
SG08	22.08976	77.71605	05-10-2024	24-07-2025	64.22	1.03	12
SG09	21.82800	78.09055	05-10-2024	24-07-2025	51.64	0.95	12

4 Discussion

4.1 Comparative Analysis of APM and Splitting Measurements

Understanding the deformation pattern is critical for studying the formation mechanisms and growth history of the CITZ region. The correlation between seismic anisotropy and geodetic measurements (APM and GPS velocity vectors) provides an indirect indicator for understanding deformation mechanisms in the crust and upper mantle. The GPS measurements pertain

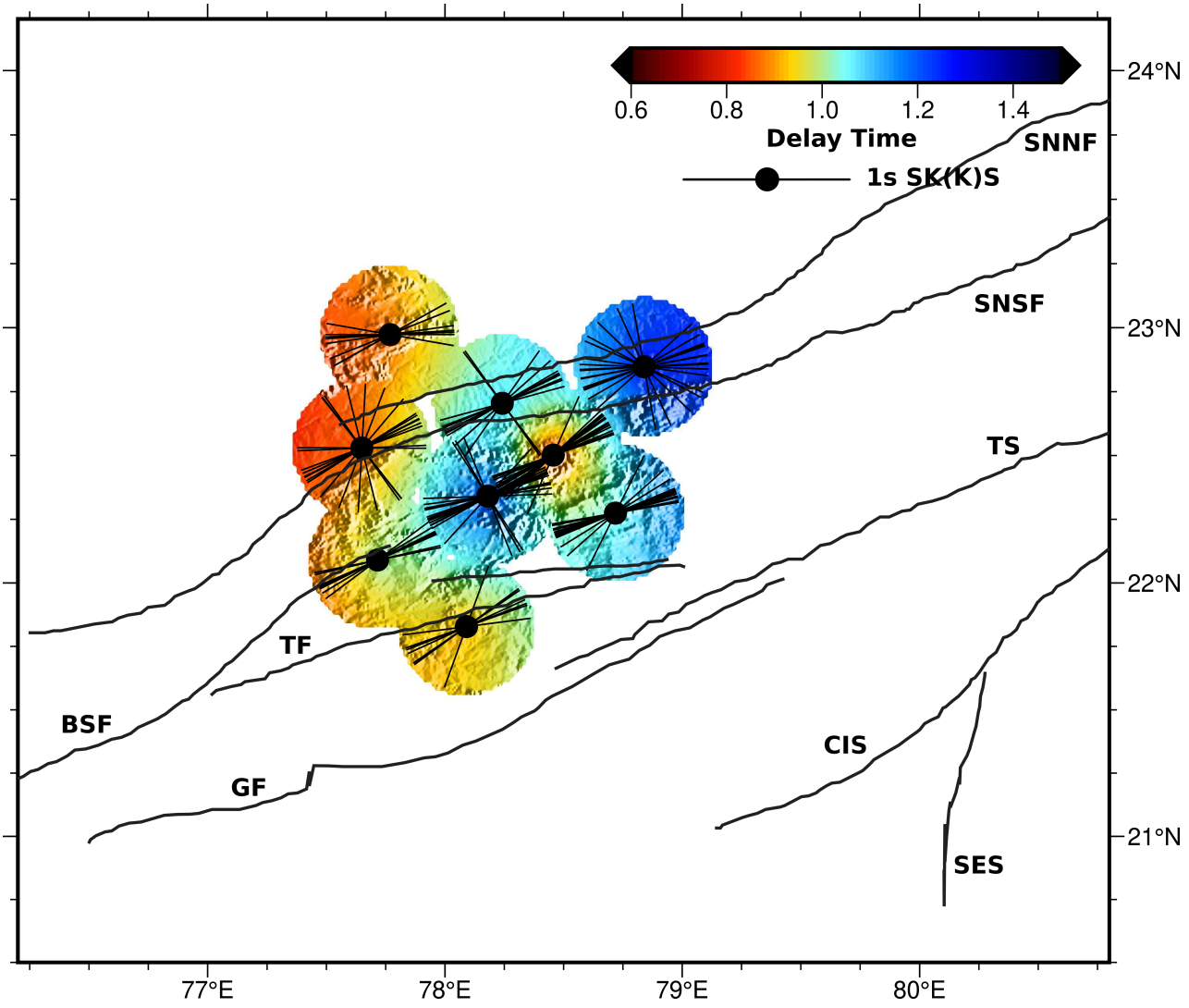


Figure 8. The tectonic map of the study area, which depicts the fast polarization direction (FPD) of individual SK(K)S splitting at each seismic station. The azimuth of the black bars denotes the individual FPDs of the obtained splitting parameters. The interpolated station-averaged split delay time at each seismic station is presented in a color-coded format to illustrate lateral variations in delay times. The black circles indicate the seismic stations used in this study.

to deformation in the upper crust (Chen et al., 2013), whereas the APM is mostly about the upper mantle (Kreemer, 2009). The discrepancies between SK(K)S-derived FPDs and GPS data imply that deformation patterns vary across the crust and upper mantle. The absolute difference between FPDs and APM direction accounts for frozen-in lithospheric anisotropy and mantle flow pattern related to shaearing of the asthenosphere at the base of lithospheric plate. We combine our SK(K)S wave splitting measurements with prior GPS velocity vectors (Jade et al., 2017), and APM velocity vectors. Figure 9 shows the station-averaged splitting parameters together with APM and GPS velocities throughout the study area, highlighting notable similarities and differences across GPS, APM velocities, and SK(K)S splitting data. GPS velocities align in a NE-SW direction, indicating that the northward movement of the Indian plate primarily affects crust motion in the study area (Figure 9). The GPS measurements and their comparison with the APM (Mahesh et al., 2012; Jade et al., 2017), show that the interior of the Indian plate, including areas influenced by the Narmada-Son lineament or other faults, exhibits no significant current deformation, and the lithosphere behaves as a rigid block. A minor variance in FPD and APM (up to 10°) is noted at seismic sites SG01, SG02, SG05, SG07, and SG09 (Figure 10), indicating the predominance of asthenospheric flow. The significant absolute differences between station-averaged FPD and APM direction in the western region (26° at SG06 and 12° at SG08) and in the eastern region (16° at SG04 and 19° at SG03) indicate the influence of ancient orogenic events from the Mesoproterozoic era (Deshmukh and Prabhakar, 2020). The CITZ may act as a channel for lateral flow within the asthenosphere. This flow could have contributed to anisotropy signatures that left significant imprints in the lithosphere, revealing varying patterns of crustal and upper mantle deformation. The variations in FPDs across different stations imply varied orientations of stress and strain within the region, highlighting the historical shifts in tectonic stress fields.

4.2 Anisotropic Sources and Geodynamic Implications

The SK(K)S-derived splitting δt at each station ranges from 0.74 to 1.4 seconds, demonstrating upper mantle heterogeneity resulted from substantial deformation in the study region. SK(K)S splitting measurements at any seismic station provide the integrated seismic anisotropy of the crust and upper mantle, which serves as an indicator of overall deformation caused by contemporary mantle flow and the prior tectonic history of the region. The origin of the anisotropy in SK(K)S splitting studies is commonly thought to originate in the upper mantle given the dominance of the dislocation creep deformation mechanisms there, which creates LPO of the intrinsically anisotropic minerals olivine and orthopyroxene. Typically, olivine aligned along the shearing direction is considered to be the major contributor to mantle anisotropy (Silver, 1996). Crustal anisotropy (Silver and Chan, 1991; Boness and Zoback, 2006), anisotropy in the transition zone (Fouch and Rondenay, 2006), and anisotropy in the D" layer (Vinnik et al., 1995; Kendall and Silver, 1996; Garnero and Lay, 1997) of the lower mantle also contribute to the measured SK(K)S wave splitting, but their potential contribution is usually smaller in comparison to the upper mantle anisotropy. Seismological and petrological findings suggest that most of the anisotropy is limited to the olivine stability field (i.e., down to about 400 km depth) and is most prominent above about 200 km depth (Karato, 1987; Meade et al., 1995).

Typical splitting delay time values for crustal regions documented so far do not exceed 0.3 s (Barruol and Mainprice, 1993), which is significantly lower than the SK(K)S-derived average split delay times for the study region. Barruol and Mainprice

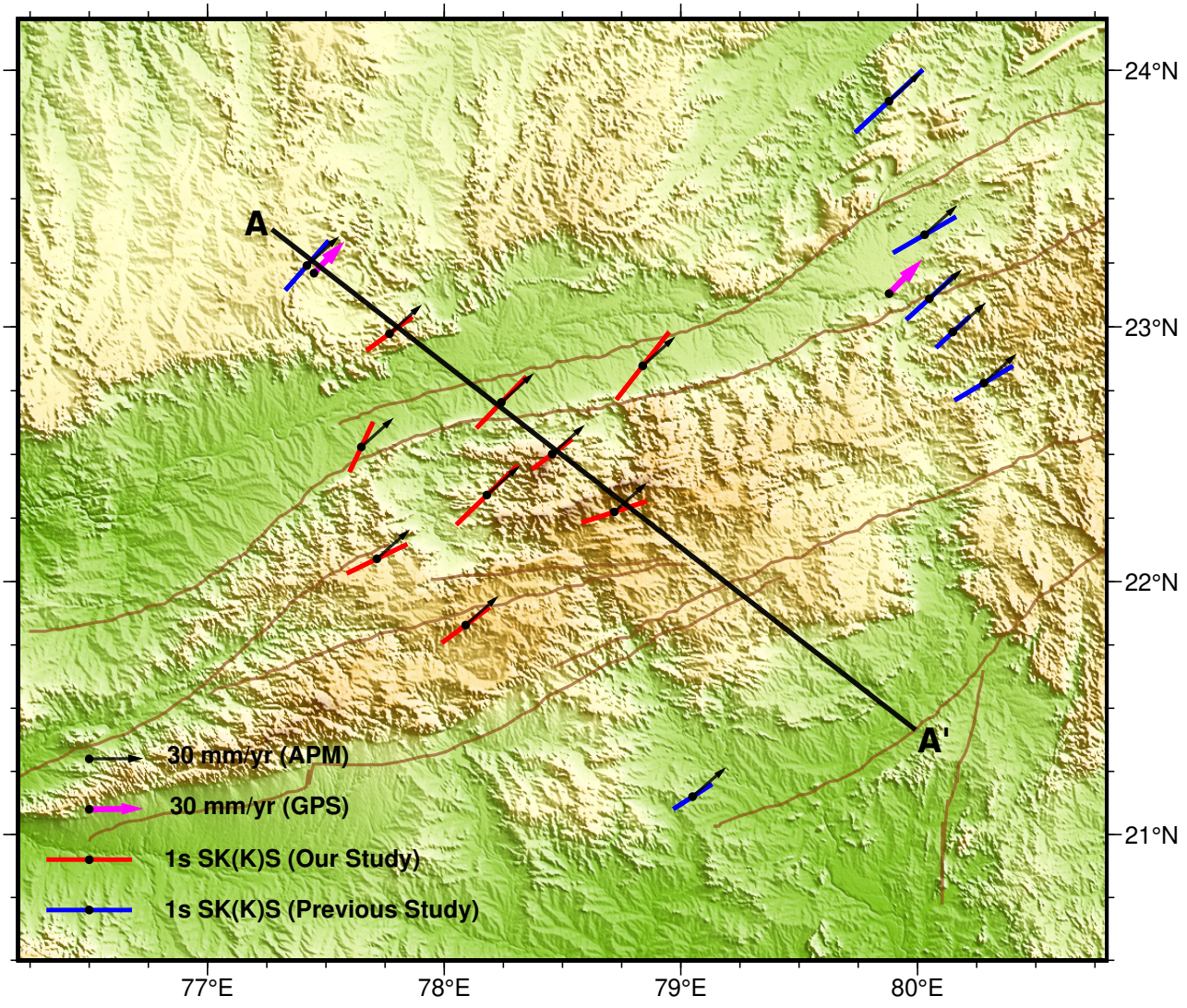


Figure 9. Lateral variation of the anisotropic and geodetic data illustrated on the tectonic and topographic map of the study region. The station-averaged splitting measurements for this study are depicted in red, whereas previous splitting measurements in adjacent regions are represented in blue. The black dots signify the location of the stations. The inclination of each bar represents the FPD, while the length denotes the δt. The GPS velocity vectors are depicted in magenta, whereas the APM direction of the Indian plate at each seismic station is represented in black.

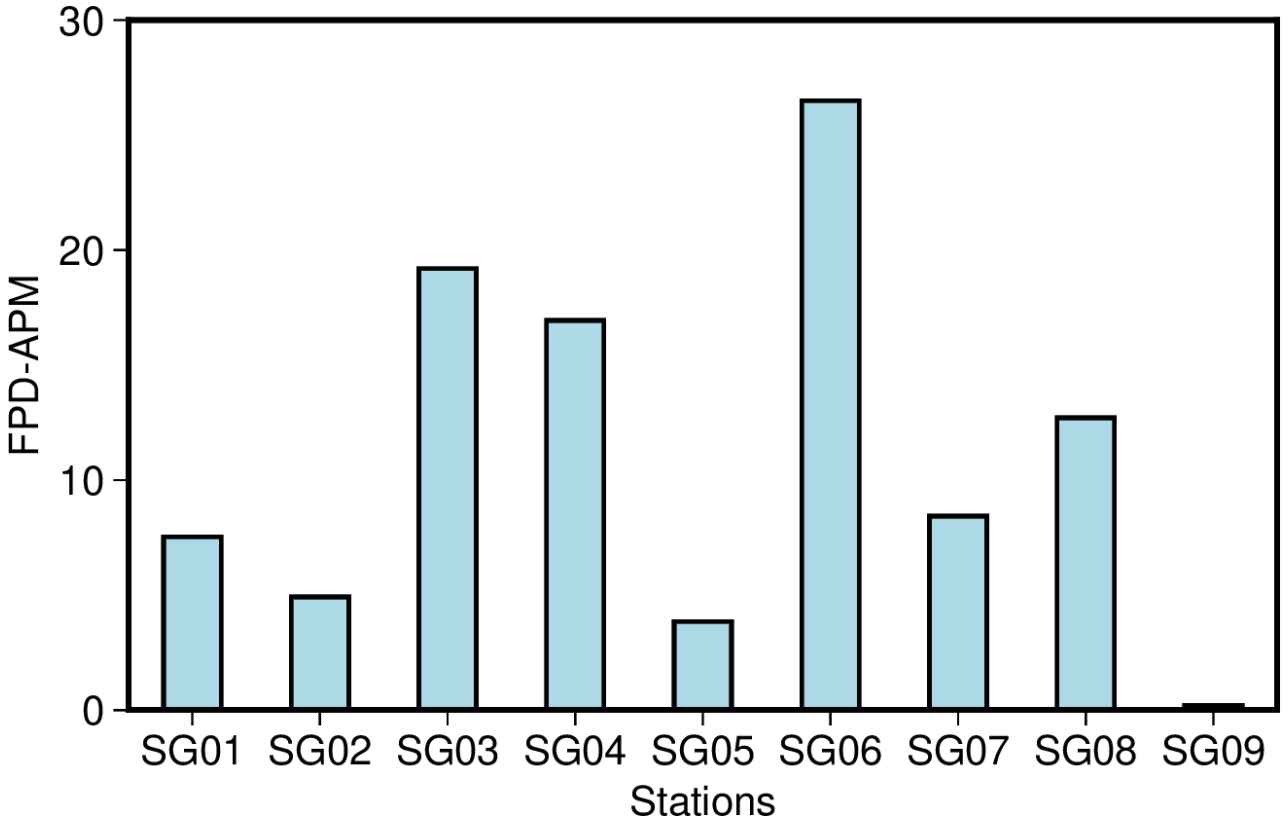


Figure 10. The bar diagram depicts the absolute difference between the station-averaged FPD for each station and the APM direction of the Indian plate, signifying the deviation of FPDs from the APM direction.

(1993) quantitatively constrained the crustal contribution to SK(K)S delay times by modeling the elastic properties of typical crustal compositions and petrofabrics and establishing that even strongly foliated crustal rocks contribute no more than 0.1 s per 10 km of anisotropic path. The measured δt values at SG02, the lowest δt (0.76 sec) at all seismic stations, exceeded expected crustal contributions, indicating a dominant mantle source. Crustal anisotropy is commonly attributed to LPO in mica-rich minerals such as biotite and amphibole, as well as SPO in cracks, fractures, and compositional layering formed during deformation (Crampin, 1984; Mainprice and Nicolas, 1989; Fouch and Rondenay, 2006; Brownlee et al., 2017). Deep seismic sounding profiles along the Hirapur-Mandla transect over the NSL restrict the Moho depth to 40-44 km beneath the study region (Murty et al., 2004; Kaila et al., 1989), with local thickening to $\sim$52 km eastwards near the Narmada paleo-rift zone (Kumar et al., 2015a). A typical crustal thickness of $\sim$40 km under the CITZ results in a maximum crustal contribution of $\sim$0.3-0.4 s. Additionally, the entire crust is not uniformly anisotropic; only the mid-to-lower crust, where ductile deformation aligns amphibole and biotite crystals (Mainprice and Nicolas, 1989; Meissner et al., 2002), contributes significantly. For an approximate lower crustal anisotropic thickness of 15-30 km, the crustal contribution is 0.15-0.3 s. The remaining delay times

may reflect residual contributions from upper mantle anisotropy.

Upper mantle anisotropy is primarily attributed to the strain-induced LPO of anisotropic minerals such as olivine, orthopyroxene, and clinopyroxene, which results from the dislocation creep deformation mechanism, which is characterized by the creeping motion of crystal dislocations caused by mantle flow and tectonic stresses at plate boundaries due to past and ongoing deformations (Karato, 1987; Barruol and Mainprice, 1993; Mainprice et al., 2000). The LPO of olivine developed during deformation can be frozen into the lithosphere and retained for billions of years (Silver and Chan, 1991; Savage, 1999). This fossilized anisotropy can influence SK(K)S delay times regardless of the plate's subsequent motion. Fresnel zone analysis demonstrate that the promising average depth of anisotropy beneath the study region is at 235 km depth (indicated by the star in Figure 11). This depth range is consistent with a sub-lithospheric, asthenospheric source of anisotropy, suggesting that mantle flow at asthenospheric depths, rather than frozen lithospheric fabric, is the primary driver of the observed shear-wave splitting. However, pure asthenospheric flow is also insufficient on its own, because if the anisotropy were entirely asthenospheric (i.e., purely APM-driven), the FPDs would be expected to align uniformly and exactly with the APM direction across all stations (Vinnik et al., 1995), which is not the case. At 5 out of 9 stations, angular deviations between FPD and APM exceed 10°, reaching up to $\sim$35° at stations located near major geological boundaries of the CITZ. Seismological studies have indicated that the deviation in the FPD from the APM direction may reflect deformation originating within the lithosphere, particularly in regions with layered anisotropy corresponding to multiple deformation episodes (Link and Rümpker, 2023).

The lithosphere-asthenosphere boundary (LAB) beneath central India has a non-uniform depth profile (Kumar et al., 2013; Maurya et al., 2016; Kumar and Mohanty, 2025), characterized by undulations that could indicate tectonic and compositional variations across the region (Supplementary Figure S3). The undulating LAB may influence seismic wave propagation, resulting in diverse anisotropic signatures that depend on the boundary's depth and shape. In shallower LAB zones, mantle flow may have a greater direct influence on the anisotropic fabric, contributing to SWS with FPDs aligned with recent tectonic stress directions or mantle convection patterns (Bormann et al., 1996). The SG03 and SG06 seismic stations may be located in locations with thicker lithosphere (180-200 km of LAB thickness), where fossilized fabric from past tectonic events could influence anisotropy (Chagas de Melo and Assumpcão, 2018; Yang et al., 2017). In the northeast of the study region, the stations JBP to LLP also exhibit a distinct splitting trend, demonstrating that lithospheric thickness is almost proportionate to δt (Roy et al., 2024). This trend is corroborated by Moho depth estimates from the passive seismological study of the Narmada Paleo rift (Kumar et al., 2015a), which show a duplex structure of the Moho discontinuity, characterized by a thicker crust (surpassing 52 km) within the rift zone than in surrounding regions. Regions with higher lithospheric thickness may have seen more intense deformation, especially in active subduction and collision zones. Figure 8 shows that the central region of the study area has seen many stages of deformation resulting in higher δts. Stations SG07, SG06, and SG09, located within or near DVP, have lower δt values. The observed characteristics at these stations may be associated with mantle plume upwelling in the upper Cretaceous to early Paleocene (Krishnamurthy, 2020). In addition to lower δt, we also found 6 null measurements at stations near the mantle plume activity, four at SG02 and two at SG09 seismic station. Station SG02 has the lowest δt value (0.74 sec). The

lower δt (0.74 sec) and 4 null measurements in the Pachmarhi region (SG02 seismic station) could be attributable to significant magmatism during the Cretaceous era in the Narmada and Tapti graben zones, as evidenced by the presence of dykes near the SG02 station (Shukla et al., 2022). The 2D gravity modeling of the Satpura Gondwana basin (Singh et al., 2015) additionally demonstrated that the basin functioned as a drop-down basin before being uplifted to its current elevation by late Cretaceous Deccan volcanism. Station SG09 is located close to the DVP. The lower δt (0.95 sec) and 2 null measurements at SG09 may be linked to mantle plume upwelling during the upper Cretaceous to early Paleocene (Krishnamurthy, 2020). Anisotropic fabrics beneath SG04 and SG05 seismic stations show preserved mantle deformation from ancient subduction zones, as shown by elevated δt values.

The SG08 seismic station, located near the Tapti Fault, exhibits a fault-parallel FPD, suggesting uniaxial compression and a fault that may extend to greater depths (Savage, 1999), possibly reaching the lithospheric mantle. The Tapti fault is a major east-west trending structure located in central India (Chakraborty and Ghosh, 2005). The fault-parallel alignment of FPD suggests that seismic anisotropy in this area is structurally controlled by the fault, implying that it serves as a weak lithospheric zone influencing upper mantle deformation (Kumar et al., 2007). Fault-parallel FPD alignment suggests that the Tapti fault, which has undergone several reactivation stages in conjunction with present-day stress fields, has pre-existing weaknesses in the crust and mantle (Copley et al., 2014), and that the fault may be a deep-seated lithospheric-scale fault.

We created a conceptual tectonic model (Figure 12) to understand how CITZ formation over time affects deformation and impacted the FPD orientation and δts values. The model is made along AA', which stretches from a region of low deformation in the northwest to an active subduction zone in the southeast. This is corroborated by variations in SK(K)S-derived FPDs and δts. Stations SG01 and SG03 have higher δts compared to BHPL and SG07, indicating a greater impact from subduction-related deformation (Deshmukh and Prabhakar, 2020). The lower δt at station SG02 is attributed to significant magmatism during the Cretaceous period mantle plume activity, as shown by the existence of dykes in the Pachmarhi region. The mantle plume is inducing localized alterations in lithospheric structure and seismic anisotropy. The low δt at NGP is likely due to its considerable distance from the active subduction zone. Station SG03 exhibits significant variability in FPD and APM, reflecting a tectonically complex mantle deformation zone linked to the inherited frozen lithospheric anisotropy resulting from previous convergence and collisional orogeny beneath the CITZ region, in addition to the current APM direction of the Indian plate. The recent tectonic evolution model of the CITZ (Deshmukh and Prabhakar, 2020, and references therein) proposes the likelihood of double-sided subduction, which accounts for the present-day tectonic framework of the CITZ region. This involves the processes of slab roll-off and subduction polarity reversal between the northern and southern Indian cratons, characterized by an initial southward subduction of the northern Indian craton, followed by a reversal of the subduction polarity. However, the current investigation of seismic anisotropy does not provide confirmation of the slab break-off hypothesis. To obtain comprehensive information regarding the detached remnants slab, slab break-off, and polarity reversal, additional seismological investigations (such as seismic tomography, splitting intensity tomography, receiver function analysis, etc.) are required to

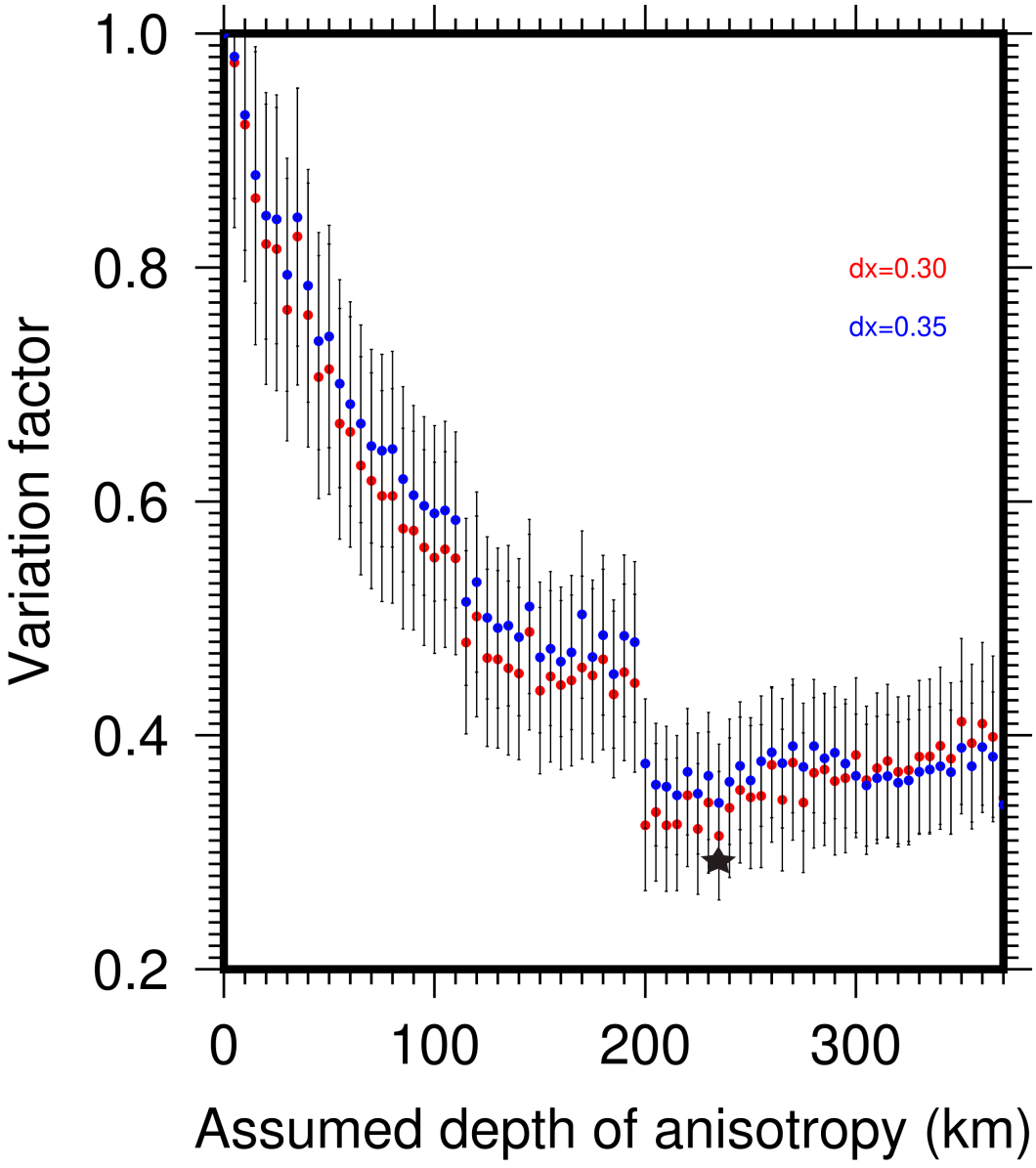


Figure 11. Depiction of the variation factor as a function of the presumed depth of anisotropy, calculated for block sizes of 0.30° and 0.35°. The variation factor is calculated as the weighted sum of the circular mean of the fast polarization directions and the arithmetic mean of the delay times.

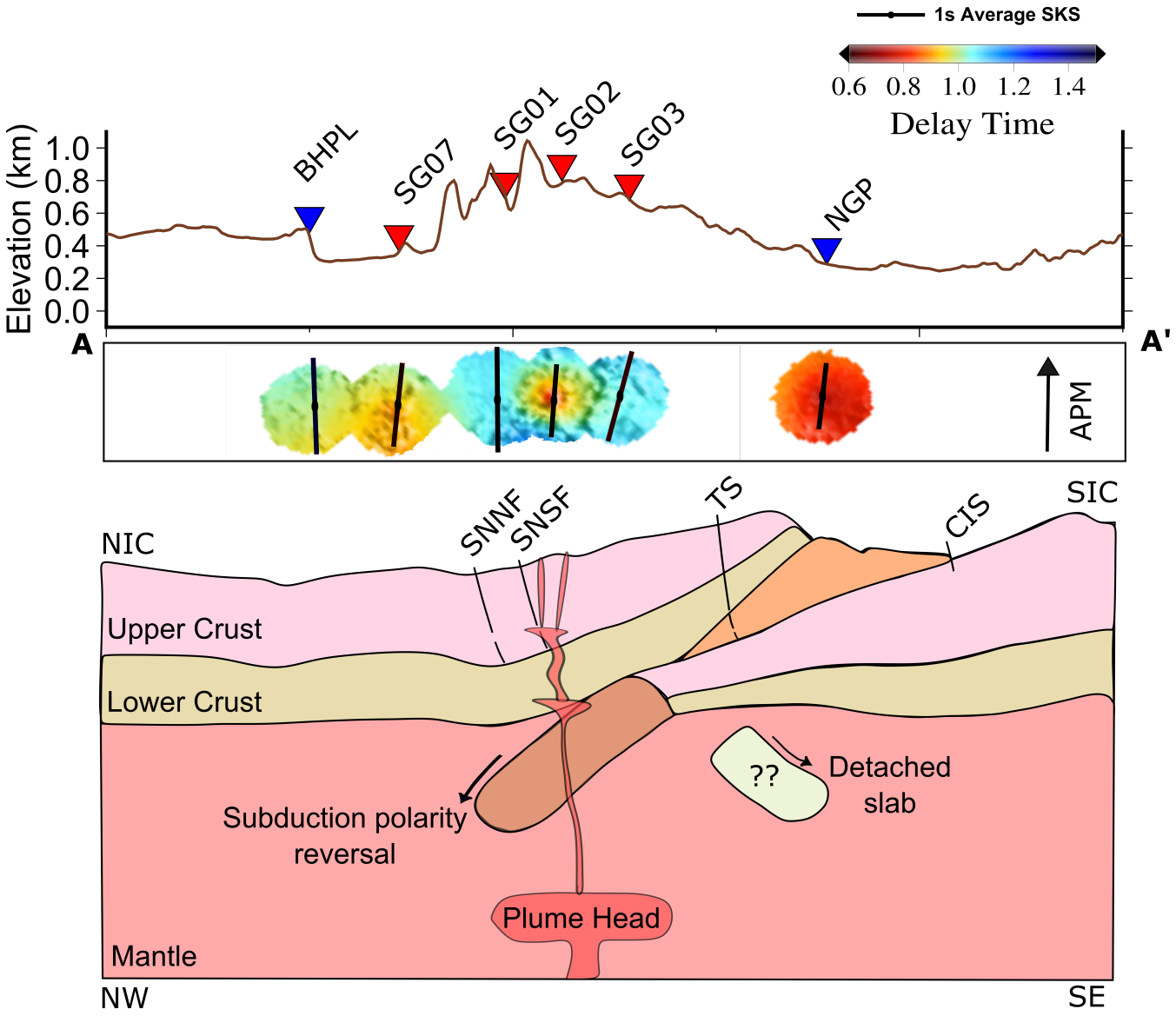


Figure 12. A hypothetical model (not to scale) depicting all tectonic events that have influenced the formation of CITZ over time and affected the FPD alignment and δts. The model is built along AA' profile, extending from a low deformation area in the northwest to an active subduction zone in the southeast, as illustrated in Figure 11. The elevation profile at the top illustrates the present-day topography along the A-A' transect, showing seismic station locations from the present study (red triangles) and previous studies (blue triangles). The middle panel denotes the average splitting measurements; bar length is proportional to delay times, and orientation indicates fast polarisation directions along with the interpolated split delay time at each station, which is displayed in a color-coded style to distinctly illustrate lateral variations in split delay times. The schematic cross-section in the bottom panel depicts the Mesoproterozoic collisional era ($\sim$1.55-0.85 Ga), specifically capturing the subduction polarity reversal and N-directed subduction of the SIC and possible subduction polarity reversal, as well as mantle plume activity during the late Cretaceous to early Paleocene. The subduction model representing the Mesoproterozoic collisional stage ($\sim$1.55-1.10 Ga) is modified from Deshmukh and Prabhakar (2020) and Mall et al. (2008), while the plume upwelling is additionally demonstrated by Shukla et al. (2022). APM: Absolute Plate Motion, NIC: North Indian Craton, SIC: South Indian Craton.

elucidate the detailed tectonic framework of the CITZ and the surrounding adjacent regions.

5 Conclusions

This study focuses on mantle deformation beneath the CITZ, supported by SWS data from the Satpura Gondwana region. The key implications of our study are as follows:

1. The SK(K)S splitting results indicate the presence of a significant anisotropic fabric beneath the studied area.

2. Fresnel zone analysis shows that 235 km is a promising average depth of anisotropy, consistent with a sub-lithospheric source of anisotropy, implying that mantle flow at asthenospheric depths, rather than frozen lithospheric fabric, is the primary driver of the observed seismic anisotropy.

3. The FPDs generally vary from NNE-SSW to ENE-WSW, deviating from the APM direction of the Indian plate ($\sim$48°). The deviation of the averaged FPD orientation from the APM direction of the Indian plate at each seismic station suggests that the inferred deformation pattern is caused by a combination of frozen lithospheric deformation and sub-lithospheric mantle dynamics, rather than asthenospheric flow caused by Indian plate motion. The presence of preserved anisotropic signatures, which have been retained due to the orogenic processes associated with the convergence and collisions of the Northern Bundelkhand and Deccan protocontinents during the evolution of CITZ until the early Neoproterozoic.

4. The lower splitting delay times (δt $<$ 1s) for seismic stations SG02, SG06, SG07, and SG09 can be attributed to plume upwelling during the late Cretaceous to early Paleocene, as indicated by the presence of dykes or their vicinity to the Deccan Trap.

5. The obtained FPD orientation at seismic station (SG08), situated near the Tapti Fault, is aligned with the fault's strike. This suggests that the fault is deep-seated, potentially extending to the lithospheric mantle, and that seismic anisotropy in this area is structurally influenced by the fault, indicating its role as a weak lithospheric zone impacting upper mantle deformation.

6. Variations in splitting patterns indicate the presence of a two- or multilayer anisotropic fabric. However, modeling two layers of anisotropy requires broad azimuthal coverage and substantial splitting measures, both of which are missing from all stations in our dataset. As a result, we have decided not to proceed with two-layer anisotropy modeling.

Code and data availability. The SplitLab code used to perform SK(K)S phase splitting measurements is available under a General Public License (GPL) at https://github.com/IPGP/splitlab. The waveform data used in this investigation are available on request from the corresponding author.

Author contributions. Nitarani Bishoyi: Conceptualization, Methodology, Software, Data curation, Visualization, Validation, Writing-Original draft. Arun Kumar Dubey: Data collection, Validation, Writing-Reviewing and Editing. Ashwani Kant Tiwari: Data Collection, Supervision, Conceptualization, Methodology, Visualization, Validation, Resources, Writing-Reviewing and Editing

Competing interests. The authors declare that they have no conflict of interest.

Acknowledgements. This study was funded by the Indian Institute of Science Education and Research Bhopal. We are thankful to our group members Rahul Kumar, and Rishabh Tripathi for their excellent support during fieldwork and the smooth functioning of the project. We used Generic Mapping Tools (Wessel et al., 2013, 2019) to create all figures except Figures 5, 6, and 12. We thank associate editor Irene Bianchi and anonymous reviewers for their valuable comments and suggestions, which helped us to improve the paper substantially.

References

Acharya, S. (1997). Evolutionary characters of the Gondwanic Indian crust. *Indian Minerals*, 51:1–24. https://doi.org/10.1101/184663.

Acharyya, S. (2003). The nature of Mesoproterozoic Central Indian Tectonic Zone with exhumed and reworked older granulites. *Gondwana Research*, 6(2):197–214. https://doi.org/10.1016/s1342-937x(05)70970-9.

Altamimi, Z., Métivier, L., Rebischung, P., Collilieux, X., Chanard, K., and Barnéoud, J. (2023). ITRF2020 Plate Motion Model. *Geophysical Research Letters*, 50(24). http://dx.doi.org/10.1029/2023GL106373.

Barruol, G. and Mainprice, D. (1993). A quantitative evaluation of the contribution of crustal rocks to the shear-wave splitting of teleseismic SKS waves. *Physics of the Earth and Planetary Interiors*, 78(3-4):281–300. https://doi.org/10.1016/0031-9201(93)90161-2.

Barruol, G., Silver, P. G., and Vauchez, A. (1997). Seismic anisotropy in the eastern United States: Deep structure of a complex continental plate. *Journal of Geophysical Research: Solid Earth*, 102(B4):8329–8348. http://dx.doi.org/10.1029/96JB03800.

Bhandari, A., Chandra Pant, N., Bhowmik, S. K., and Goswami, S. (2011). 1.6 Ga ultrahigh-temperature granulite metamorphism in the Central Indian Tectonic Zone: insights from metamorphic reaction history, geothermobarometry and monazite chemical ages. *Geological Journal*, 46(2-3):198–216. https://doi.org/10.1002/gj.1221.

Bhowmik, S. K., Wilde, S. A., Bhandari, A., Pal, T., and Pant, N. C. (2012). Growth of the Greater Indian Landmass and its assembly in Rodinia: geochronological evidence from the Central Indian Tectonic Zone. *Gondwana Research*, 22(1):54–72. https://doi.org/10.1016/j.gr.2011.09.008.

Bhukta, K., Khan, P. K., and Mandal, P. (2018). Upper mantle anisotropy inferred from shear wave splitting beneath the Eastern Indian Shield region. *Geoscience Frontiers*, 9(6):1911–1920. https://doi.org/10.1016/j.gsf.2017.12.003.

Biswal, S., Kumar, S., Roy, S. K., Kumar, M. R., Mohanty, W., Parija, M. P., and Paul, A. (2020). Upper mantle anisotropy beneath the Western Segment, NW Indian Himalaya, using shear wave splitting. *Lithosphere*, 2020(1):8856812. https://doi.org/10.2113/2020/8856812.

Boness, N. L. and Zoback, M. D. (2006). A multiscale study of the mechanisms controlling shear velocity anisotropy in the San Andreas Fault Observatory at Depth. *Geophysics*, 71(5):F131–F146. http://dx.doi.org/10.1190/1.2231107.

Bora, S. and Kumar, S. (2015). Geochemistry of biotites and host granitoid plutons from the Proterozoic Mahakoshal Belt, central India tectonic zone: implication for nature and tectonic setting of magmatism. *International Geology Review*, 57(11-12):1686–1706. https://doi.org/10.1080/00206814.2015.1032372.

Bormann, P., Grünthal, G., Kind, R., and Montag, H. (1996). Upper mantle anisotropy beneath central Europe from SKS wave splitting: Effects of absolute plate motion and lithosphere-asthenosphere boundary topography? *Journal of Geodynamics*, 22(1-2):11–32. https://doi.org/10.1016/0264-3707(96)00014-2.

Bowman, J. R. and Ando, M. (1987). Shear-wave splitting in the upper-mantle wedge above the Tonga subduction zone. *Geophysical Journal International*, 88(1):25–41. https://doi.org/10.1111/j.1365-246x.1987.tb01367.x.

Brownlee, S. J., Schulte-Pelkum, V., Raju, A., Mahan, K., Condit, C., and Orlandini, O. F. (2017). Characteristics of deep crustal seismic anisotropy from a compilation of rock elasticity tensors and their expression in receiver functions. *Tectonics*, 36(9):1835–1857. http://dx.doi.org/10.1002/2017TC004625.

Chagas de Melo, B. and Assumpcão, M. a. (2018). Mantle anisotropy and asthenospheric flow around cratons in southeastern South America. *Geophysical Journal International*, 215(1):494–506. http://dx.doi.org/10.1093/gji/ggy288.

Chakraborty, C. and Ghosh, S. K. (2005). Pull-apart origin of the Satpura Gondwana basin, central India. *Journal of earth system science*, 114:259–273. https://doi.org/10.1007/bf02702949.

Chattopadhyay, A., Chatterjee, A., Das, K., and Sarkar, A. (2017). Neoproterozoic transpression and granite magmatism in the Gavilgarh-Tan Shear Zone, central India: Tectonic significance of U-Pb zircon and U-Th-total Pb monazite ages. *Journal of Asian Earth Sciences*, 147:485–501. https://doi.org/10.1016/j.jseaes.2017.08.018.

Chen, Y., Zhang, Z., Sun, C., and Badal, J. (2013). Crustal anisotropy from Moho converted Ps wave splitting analysis and geodynamic implications beneath the eastern margin of Tibet and surrounding regions. *Gondwana Research*, 24(3-4):946–957. https://doi.org/10.1016/j.gr.2012.04.003.

Cochran, E. S., Vidale, J. E., and Li, Y. (2003). Near-fault anisotropy following the Hector Mine earthquake. *Journal of Geophysical Research: Solid Earth*, 108(B9). http://dx.doi.org/10.1029/2002JB002352.

Copley, A., Mitra, S., Sloan, R. A., Gaonkar, S., and Reynolds, K. (2014). Active faulting in apparently stable peninsular India: Rift inversion and a Holocene-age great earthquake on the Tapti Fault. *Journal of Geophysical Research: Solid Earth*, 119(8):6650–6666. https://doi.org/10.1002/2014jb011294.

Crampin, S. (1984). Effective anisotropic elastic constants for wave propagation through cracked solids. *Geophysical Journal International*, 76(1):135–145. http://dx.doi.org/10.1111/j.1365-246X.1984.tb05029.x.

Deshmukh, T. and Prabhakar, N. (2020). Linking collision, slab break-off and subduction polarity reversal in the evolution of the Central Indian Tectonic Zone. *Geological Magazine*, 157(2):340–350. https://doi.org/10.1017/s0016756819001419.

Eakin, C. M., Rychert, C. A., and Harmon, N. (2018). The Role of Oceanic Transform Faults in Seafloor Spreading: A Global Perspective From Seismic Anisotropy. *Journal of Geophysical Research: Solid Earth*, 123(2):1736–1751. http://dx.doi.org/10.1002/2017JB015176.

Eakin, C. M., Wirth, E. A., Wallace, A., Ulberg, C. W., Creager, K. C., and Abers, G. A. (2019). SKS Splitting Beneath Mount St. Helens: Constraints on Subslab Mantle Entrainment. *Geochemistry, Geophysics, Geosystems*, 20(8):4202–4217. http://dx.doi.org/10.1029/2019GC008433.

Fouch, M. J. and Rondenay, S. (2006). Seismic anisotropy beneath stable continental interiors. *Physics of the Earth and Planetary Interiors*, 158(2-4):292–320. http://dx.doi.org/10.1016/j.pepi.2006.03.024.

Fröhlich, Y., Grund, M., and Ritter, J. R. R. (2024). Lateral and vertical variations of seismic anisotropy in the lithosphere–asthenosphere system underneath Central Europe from long-term splitting measurements. *Geophysical Journal International*, 239(1):112–135. http://dx.doi.org/10.1093/gji/ggae245.

Gao, S. S. and Liu, K. H. (2012). AnisDep: A FORTRAN program for the estimation of the depth of anisotropy using spatial coherency of shear-wave splitting parameters. *Computers amp; Geosciences*, 49:330–333. http://dx.doi.org/10.1016/j.cageo.2012.01.020.

Garnero, E. J. and Lay, T. (1997). Lateral variations in lowermost mantle shear wave anisotropy beneath the north Pacific and Alaska. *Journal of Geophysical Research: Solid Earth*, 102(B4):8121–8135. http://dx.doi.org/10.1029/96JB03830.

Hou, G., Santosh, M., Qian, X., Lister, G. S., and Li, J. (2008). Tectonic constraints on 1.3˜ 1.2 Ga final breakup of Columbia supercontinent from a giant radiating dyke swarm. *Gondwana Research*, 14(3):561–566. https://doi.org/10.1016/j.gr.2008.03.005.

Jade, S., Shrungeshwara, T., Kumar, K., Choudhury, P., Dumka, R. K., and Bhu, H. (2017). India plate angular velocity and contemporary deformation rates from continuous GPS measurements from 1996 to 2015. *Scientific reports*, 7(1):11439. https://doi.org/10.1038/s41598-017-11697-w.

Jana, N., Singh, A., Tiwari, A. K., Eken, T., Singh, A., Singh, C., and Shankar, U. (2021). Seismic anisotropy and mantle deformation beneath Eastern Ghats Mobile Belt using direct-S waves. *Precambrian Research*, 360:106215. https://doi.org/10.1016/j.precamres.2021.106215.

Kaila, K. and Krishna, V. (1992). Deep seismic sounding studies in India and major discoveries. *Current science (Bangalore)*, 62(1-2):117–154. https://doi.org/10.3809/jvirtex.2003.00080.

Kaila, K., Murty, P., and Mall, D. (1989). The evolution of the Vindhyan basin vis-à-vis the Narmada-Son lineament, central India, from deep seismic soundings. *Tectonophysics*, 162(3-4):277–289. http://dx.doi.org/10.1016/0040-1951(89)90249-7.

Kanaujia, J., Mitra, S., Gupta, S. C., and Sharma, M. L. (2019). Crustal anisotropy from shear-wave splitting of local earthquakes in the Garhwal Lesser Himalaya. *Geophysical Journal International*, 219(3):2013–2033. https://doi.org/10.1093/gji/ggz404.

Kanaujia, J. and Surve, G. (2024). Upper mantle deformation beneath the northeastern part of Indian plate from shear-wave splitting analysis. *Geo-Marine Letters*, 44(1):1. https://doi.org/10.21203/rs.3.rs-3127002/v1.

Karato, S.-i. (1987). *Seismic anisotropy due to lattice preferred orientation of minerals: Kinematic or dynamic?*, page 455–471. American Geophysical Union. http://dx.doi.org/10.1029/GM039p0455.

Kendall, J.-M. and Silver, P. G. (1996). Constraints from seismic anisotropy on the nature of the lowermost mantle. *Nature*, 381(6581):409–412. http://dx.doi.org/10.1038/381409a0.

Kreemer, C. (2009). Absolute plate motions constrained by shear wave splitting orientations with implications for hot spot motions and mantle flow. *Journal of Geophysical Research: Solid Earth*, 114(B10). https://doi.org/10.1029/2009jb006416.

Krishnamurthy, P. (2020). The Deccan Volcanic Province (DVP), India: a review: Part 1: Areal extent and distribution, compositional diversity, flow types and sequences, stratigraphic correlations, dyke swarms and sills, petrography and mineralogy. *Journal of the Geological Society of India*, 96(1):9–35. https://doi.org/10.1007/s12594-020-1521-1.

Kumar, M., Singh, A., Kumar, N., and Sarkar, D. (2015a). Passive seismological imaging of the Narmada paleo-rift, central India. *Precambrian Research*, 270:155–164. https://doi.org/10.1016/j.precamres.2015.09.013.

Kumar, M. R. and Singh, A. (2008). Evidence for plate motion related strain in the Indian shield from shear wave splitting measurements. *Journal of Geophysical Research: Solid Earth*, 113(B8). https://doi.org/10.1029/2007jb005128.

Kumar, P. and Mohanty, W. K. (2025). Evaluating the Lithospheric Structure and Regional/Residual Bouguer Anomalies in Peninsular India Through Potential Field Modeling and Thermal Analysis. *Journal of Geophysical Research: Solid Earth*, 130(4). http://dx.doi.org/10.1029/2024JB029341.

Kumar, P., Ravi Kumar, M., Srijayanthi, G., Arora, K., Srinagesh, D., Chadha, R., and Sen, M. K. (2013). Imaging the lithosphere-asthenosphere boundary of the Indian plate using converted wave techniques. *Journal of Geophysical Research: Solid Earth*, 118(10):5307–5319. https://doi.org/10.1002/jgrb.50366.

Kumar, P., Yuan, X., Kumar, M. R., Kind, R., Li, X., and Chadha, R. (2007). The rapid drift of the Indian tectonic plate. *Nature*, 449(7164):894–897. https://doi.org/10.1038/nature06214.

Kumar, V. P., Prakasam, K., Rai, S., and Gupta, S. (2015b). Upper-mantle anisotropy beneath the south Indian Shield: Influenced by ancient and recent Earth processes. *Lithosphere*, 7(2):108–116. https://doi.org/10.1130/l405.1.

Li, Z.-X., Bogdanova, S., Collins, A., Davidson, A., De Waele, B., Ernst, R., Fitzsimons, I., Fuck, R., Gladkochub, D., Jacobs, J., et al. (2008). Assembly, configuration, and break-up history of Rodinia: a synthesis. *Precambrian research*, 160(1-2):179–210. https://doi.org/10.1016/j.precamres.2009.01.012.

Link, F. and Rümpker, G. (2023). Shear-Wave Splitting Reveals Layered-Anisotropy Beneath the European Alps in Response to Mediterranean Subduction. *Journal of Geophysical Research: Solid Earth*, 128(9). http://dx.doi.org/10.1029/2023JB027192.

Liu, K. H. and Gao, S. S. (2011). Estimation of the Depth of Anisotropy Using Spatial Coherency of Shear-Wave Splitting Parameters. *Bulletin of the Seismological Society of America*, 101(5):2153–2161. http://dx.doi.org/10.1785/0120100258.

Long, M. D. and Silver, P. G. (2009). Shear Wave Splitting and Mantle Anisotropy: Measurements, Interpretations, and New Directions. *Surveys in Geophysics*, 30(4-5):407–461. http://dx.doi.org/10.1007/s10712-009-9075-1.

Mahesh, P., Catherine, J., Gahalaut, V., Kundu, B., Ambikapathy, A., Bansal, A., Premkishore, L., Narsaiah, M., Ghavri, S., Chadha, R., et al. (2012). Rigid Indian plate: constraints from GPS measurements. *Gondwana Research*, 22(3-4):1068–1072. https://doi.org/10.1016/j.gr.2012.01.011.

Mainprice, D., Barruol, G., and Ismaïl, W. B. (2000). *The Seismic anisotropy of the Earth's mantle: From single crystal to polycrystal*, page 237–264. American Geophysical Union. http://dx.doi.org/10.1029/GM117p0237.

Mainprice, D. and Nicolas, A. (1989). Development of shape and lattice preferred orientations: application to the seismic anisotropy of the lower crust. *Journal of Structural Geology*, 11(1-2):175–189. http://dx.doi.org/10.1016/0191-8141(89)90042-4.

Mall, D., Reddy, P., and Mooney, W. D. (2008). Collision tectonics of the Central Indian Suture zone as inferred from a deep seismic sounding study. *Tectonophysics*, 460(1-4):116–123. https://doi.org/10.1016/j.tecto.2008.07.010.

Mandal, B., Sen, M. K., and Vijaya Rao, V. (2013). New seismic images of the Central Indian Suture Zone and their tectonic implications. *Tectonics*, 32(4):908–921. https://doi.org/10.1002/tect.20055.

Maurya, S., Montagner, J., Kumar, M. R., Stutzmann, E., Kiselev, S., Burgos, G., Rao, N. P., and Srinagesh, D. (2016). Imaging the lithospheric structure beneath the Indian continent. *Journal of Geophysical Research: Solid Earth*, 121(10):7450–7468. http://dx.doi.org/10.1002/2016JB012948.

Meade, C., Silver, P. G., and Kaneshima, S. (1995). Laboratory and seismological observations of lower mantle isotropy. *Geophysical Research Letters*, 22(10):1293–1296. http://dx.doi.org/10.1029/95GL01091.

Meissner, R., Mooney, W. D., and Artemieva, I. (2002). Seismic anisotropy and mantle creep in young orogens. *Geophysical Journal International*, 149(1):1–14. http://dx.doi.org/10.1046/j.1365-246X.2002.01628.x.

Murty, A. S. N., Tewari, H. C., and Reddy, P. R. (2004). 2-D Crustal Velocity Structure Along Hirapur-Mandla Profile in Central India: An Update. *Pure and Applied Geophysics*, 161(1):165–184. http://dx.doi.org/10.1007/s00024-003-2429-6.

Naganjaneyulu, K. and Santosh, M. (2010). The Central India Tectonic Zone: a geophysical perspective on continental amalgamation along a Mesoproterozoic suture. *Gondwana Research*, 18(4):547–564. https://doi.org/10.1016/j.gr.2010.02.017.

Narula, P., Acharyya, S., and Banerjee, J. (2000). Seismotectonic atlas of India and its environs. Geological Survey of India. https://doi.org/10.56153/g19088-021-0064-6.

Paul, A., Hazarika, D., and Wadhawan, M. (2017). Shear wave splitting and crustal anisotropy in the Eastern Ladakh-Karakoram zone, northwest Himalaya. *Journal of Asian Earth Sciences*, 140:122–134. https://doi.org/10.1016/j.jseaes.2017.04.010.

Radhakrishna, B. (1989). Suspect tectono-stratigraphic terrane elements in the Indian subcontinent. *Geological Society of India*, 34(1):1–24. https://doi.org/10.17491/jgsi/1989/340101.

Radhakrishna, B. and Naqvi, S. (1986). Precambrian continental crust of India and its evolution. *The Journal of Geology*, 94(2):145–166. https://doi.org/10.1016/s0166-2635(08)70173-7.

Radhakrishna, B. and Ramakrishnan, M. (1988). Archaean-Proterozoic boundary in India. *Journal Geological Society of India*, 32(4):263–278. https://doi.org/10.17491/jgsi/1988/320401.

Rao, V. V. and Reddy, P. (2002). A Mesoproterozoic supercontinent: evidence from the Indian shield. *Gondwana Research*, 5(1):63–74. https://doi.org/10.1016/s1342-937x(05)70889-3.

Ritter, J. R. R., Frohlich, Y., Sanz Alonso, Y., and Grund, M. (2022). Short-scale laterally varying SK(K)S shear wave splitting at BFO, Germany — implications for the determination of anisotropic structures. *Journal of Seismology*, 26(6):1137–1156. http://dx.doi.org/10.1007/s10950-022-10112-w.

Rogers, J. J. and Santosh, M. (2003). Supercontinents in Earth history. *Gondwana Research*, 6(3):357–368. https://doi.org/10.1016/b978-0-12-818533-9.00018-7.

Rogers, J. J. and Santosh, M. (2009). Tectonics and surface effects of the supercontinent Columbia. *Gondwana Research*, 15(3-4):373–380. https://doi.org/10.1016/j.gr.2008.06.008.

Roy, A. and Prasad, M. H. (2003). Tectonothermal events in Central Indian Tectonic Zone (CITZ) and its implications in Rodinian crustal assembly. *Journal of Asian Earth Sciences*, 22(2):115–129. https://doi.org/10.1016/s1367-9120(02)00180-3.

Roy, S. K., Kumar, M. R., Kanaujia, J., Gupta, S., Singh, B., Mandal, P., and Srinagesh, D. (2024). Insights into the mechanisms forging seismic anisotropy in the upper mantle beneath India. *Tectonophysics*, 888:230454. https://doi.org/10.1016/j.tecto.2024.230454.

Roy, S. K., Kumar, M. R., and Srinagesh, D. (2021). Mantle deformation beneath India inferred from shear wave splitting. *Journal of the Geological Society of India*, 97:1200–1206. https://doi.org/10.1007/s12594-021-1849-1.

Roy, S. K., M., R. K., and D., S. (2014). Upper and lower mantle anisotropy inferred from comprehensive SKS and SKKS splitting measurements from India. *Earth and Planetary Science Letters*, 392:192–206. http://dx.doi.org/10.1016/j.epsl.2014.02.012.

Roy, S. K., Srinagesh, D., Saikia, D., Singh, A., and Kumar, M. R. (2012). Seismic anisotropy beneath the eastern Dharwar craton. *Lithosphere*, 4(4):259–268. https://doi.org/10.1130/l198.1.

Saltzer, R. L., Gaherty, J. B., and Jordan, T. H. (2000). How are vertical shear wave splitting measurements affected by variations in the orientation of azimuthal anisotropy with depth? *Geophysical Journal International*, 141(2):374–390. http://dx.doi.org/10.1046/j.1365-246x.2000.00088.x.

Savage, M. (1999). Seismic anisotropy and mantle deformation: what have we learned from shear wave splitting? *Reviews of Geophysics*, 37(1):65–106. https://doi.org/10.1029/98rg02075.

Shukla, G., Mallik, J., and Mondal, P. (2022). Dimension-scaling relationships of Pachmarhi dyke swarm and their implications on Deccan magma emplacement. *Tectonophysics*, 843:229602. https://doi.org/10.1016/j.tecto.2022.229602.

Silver, P. G. (1996). SEISMIC ANISOTROPY BENEATH THE CONTINENTS: Probing the Depths of Geology. *Annual Review of Earth and Planetary Sciences*, 24(1):385–432. http://dx.doi.org/10.1146/annurev.earth.24.1.385.

Silver, P. G. and Chan, W. W. (1991). Shear wave splitting and subcontinental mantle deformation. *Journal of Geophysical Research: Solid Earth*, 96(B10):16429–16454. https://doi.org/10.1029/91jb00899.

Silver, P. G. and Savage, M. K. (1994). The Interpretation of Shear-Wave Splitting Parameters In the Presence of Two Anisotropic Layers. *Geophysical Journal International*, 119(3):949–963. http://dx.doi.org/10.1111/j.1365-246X.1994.tb04027.x.

Singh, A., Jana, N., Tiwari, A. K., Eken, T., Singh, A., and Singh, C. (2019). Direct S-wave derived seismic anisotropy beneath Eastern Ghats Mobile Belt and adjacent Archean cratons: Signature of collision and rifting. In *Geophysical Research Abstracts*, volume 21. https://doi.org/10.1016/j.precamres.2021.106215.

Singh, J., Chandrakala, K., Singh, A., and Mall, D. (2015). Structure and evolution of Satpura Gondwana Basin over Central Indian Tectonic Zone: inferences from seismic and gravity data. *Jour. Indian Geophys. Union*, 19(1):39–54. https://doi.org/10.5194/egusphere-egu25-964.

Sivaram, K., Kumar, V. P., Gupta, S., Prasad, B., and Kumar, S. (2022). Upper mantle seismic anisotropy beneath the Deccan Volcanic Province and the adjacent Eastern Dharwar Craton in south Indian shield from shear wave splitting analysis. *Physics of the Earth and Planetary Interiors*, 322:106829. https://doi.org/10.1016/j.pepi.2021.106829.

Tewari, H. (2001). A tectonic model of the Narmada region. *Current Science*, 80:873–878. https://doi.org/10.5194/egusphere-egu2020-18224.

Vinnik, L., Romanowicz, B., Le Stunff, Y., and Makeyeva, L. (1995). Seismic anisotropy in the D" layer. *Geophysical Research Letters*, 22(13):1657–1660. http://dx.doi.org/10.1029/95GL01327.

Vinnik, L. P., Farra, V., and Romanowicz, B. (1989). Azimuthal anisotropy in the Earth from observations of SKS at Geoscope and NARS broadband stations. *Bulletin of the Seismological Society of America*, 79(5):1542–1558. https://doi.org/10.1029/gl016i005p00409.

Wessel, P., Luis, J. F., Uieda, L. a., Scharroo, R., Wobbe, F., Smith, W. H., and Tian, D. (2019). The generic mapping tools version 6. *Geochemistry, Geophysics, Geosystems*, 20(11):5556–5564. https://doi.org/10.1029/95eo00198.

Wessel, P., Smith, W. H., Scharroo, R., Luis, J., and Wobbe, F. (2013). Generic mapping tools: improved version released. *Eos, Transactions American Geophysical Union*, 94(45):409–410. https://doi.org/10.1029/98eo00426.

Wüstefeld, A., Bokelmann, G., Zaroli, C., and Barruol, G. (2008). SplitLab: A shear-wave splitting environment in Matlab. *Computers & Geosciences*, 34(5):515–528. https://doi.org/10.1016/j.cageo.2007.08.002.

Yang, H., Peng, H., and Hu, J. (2017). The lithospheric structure beneath southeast Tibet revealed by P and S receiver functions. *Journal of Asian Earth Sciences*, 138:62–71. https://doi.org/10.5194/egusphere-egu24-13677.

Zhao, G., Sun, M., Wilde, S. A., and Li, S. (2004). A Paleo-Mesoproterozoic supercontinent: assembly, growth and breakup. *Earth-Science Reviews*, 67(1-2):91–123. https://doi.org/10.1016/j.earscirev.2004.02.003.